

# Effective densities of soot particles and their relationships with the mixing state at an urban site of the Beijing mega-city in the winter of 2018

5 Hang LIU<sup>1,2</sup>, Xiaole PAN<sup>1</sup>, Yu WU<sup>3</sup>, Dawei Wang<sup>1</sup>, Yu TIAN<sup>1,2</sup>, Xiaoyong LIU<sup>1,4</sup>, Lu LEI<sup>1,2</sup>, Yele SUN<sup>1,2,4</sup>, Pingqing FU<sup>5</sup>, Zifa WANG<sup>1,2,4</sup>

<sup>1</sup>State Key Laboratory of Atmospheric Boundary Layer Physics and Atmospheric Chemistry, Institute of Atmospheric Physics, Chinese Academy of Sciences, Beijing, 100029, China

<sup>2</sup>University of Chinese Academy of Sciences, Beijing, 100049, China

10 <sup>3</sup>State Key Laboratory of Remote Sensing Science, Institute of Remote Sensing and Digital Earth, Chinese Academy of Sciences, No. 20 Datun Road, Beijing 100101, China

<sup>4</sup>Center for Excellence in Regional Atmospheric Environment, Chinese Academy of Science, Xiamen, 361021, China

<sup>5</sup>Institute of Surface-Earth System Science, Tianjin University, Tianjin 300072, China

15 Correspondence to: Xiaole PAN (panxiaole@mail.iap.ac.cn)

## Abstract

The effective density ( $\rho_{\text{eff}}$ ) of refractory black carbon (rBC) is a key parameter relevant to their mixing state that imposes great uncertainty in evaluating the direct radiation forcing effect. In this study, a tandem DMA-CPMA-SP2 system was used to investigate the relationship between the effective density ( $\rho_{\text{eff}}$ ) and the mixing state of rBC particles during the winter of 2018 in the Beijing mega-city. During the experiment, aerosols with a known mobility diameter ( $D_{\text{mob}}$ ) and known  $\rho_{\text{eff}}$  values (0.8, 1.0, 1.2, 1.4, 1.6, and 1.8 g/cm<sup>3</sup>) were precisely selected and measured by the SP2 to obtain their corresponding mixing states. The results showed that the  $\rho_{\text{eff}}$  well represented the morphological variation in rBC-containing particles. The rBC-containing particles changed from an irregular structure to a compact spherical structure with the increase in  $\rho_{\text{eff}}$ . A  $\rho_{\text{eff}}$  value of 1.4 g/cm<sup>3</sup> was the morphological transition point. The morphology and  $\rho_{\text{eff}}$  value of the rBC-containing particles were intrinsically related to the mass ratio of non-refractory matter to rBC ( $M_{\text{R}}$ ). As the  $\rho_{\text{eff}}$  values of the rBC-containing particles increased from 0.8 to 1.8 g/cm<sup>3</sup>, the  $M_{\text{R}}$  of the rBC-containing particles significantly increased from 2 up to 6-8, indicating that atmospheric aging processes were likely to lead to the reconstruction of more compact and regular particle shapes. During the observation period, the  $\rho_{\text{eff}}$  of majority of rBC-containing particles was smaller than the morphology transition point independent of the pollution conditions. It suggested that the major rBC-containing particles did not have a spherical structure. Simulation based on an aggregate model considering the morphological information of the particles demonstrated that absorption enhancement of rBC-containing particles could be overestimated by ~17% by using a core-shell model. This study highlights the strong

25  
30

dependence of the morphology of ambient rBC-containing particles on  $\rho_{\text{eff}}$  and will be helpful for elucidating the micro physical characteristics of rBC and reducing uncertainty in the evaluation of rBC climate effects and health risks.

## 1 Introduction

35 Refractory black carbon (rBC) is the major light absorbing aerosol in the atmosphere. It plays a vital role in the climate by influencing the radiative balance, cloud properties and glacier (Flanner et al., 2007; Ramanathan and Carmichael, 2008; Bond et al., 2013). rBC is considered to be one of the most important global warming factors (Bond et al., 2013). Additionally, as a component of PM<sub>2.5</sub> (particulate matter with an aerodynamic diameter less than 2.5  $\mu\text{m}$ ), rBC has an adverse environmental effect due to degrading visibility and harming the human respiratory system (Apte et al., 2015; Lelieveld et al., 2015; Raaschou-Nielsen et al., 2013; Dominguez-Rodriguez et al., 2015). The control of rBC emission is an immediate and win-win strategy to face climate and environmental challenges.

In the troposphere, rBC mixes with other components, such as organics, sulfate and nitrate, through condensation, coagulation, heterogenous chemistry or other complicated processes. Many studies have reported that the mixing state of rBC-containing particles greatly impacts on the absorption ability (Shiraiwa et al., 2008; Nakayama et al., 2010; Shiraiwa et al., 2010) and hygroscopicity of rBC (Zhang et al., 2008; Moteki et al., 2012; Liu et al., 2013) based on a combination of laboratory, numerical model and field measurement methods. However, debate exists among researchers. For instance, several studies (Lack et al., 2012; Wang et al., 2014; Wu et al., 2016; Wang et al., 2016) observed a large absorption enhancement of rBC caused by mixing with the coating material, whereas other studies found negligible absorption enhancement (Cappa et al., 2012; Lan et al., 2013). Liu et al. (2017) proposed that the mixing structure of rBC-containing particles depended on the proportion of coating material. When coating materials are insufficient to encapsulate rBC, they tend to attach to it and provide little absorption enhancement. Sufficient coating materials will change rBC-containing particles to a core-shell structure and significantly contribute to light absorption. Thus, the morphology of rBC-containing particles needs to be further studied to minimize the error in the estimation of rBC's absorption enhancement effect. Moreover, the morphology of rBC-containing particles causes uncertainty in evaluation of the dose deposited in the respiratory system and thus in health risk estimations (Londahl et al., 2008; Alfoldy et al., 2009).

Laboratory inspection using transmission electron microscopy (TEM) can provide visual evidence of and information on the morphology of rBC-containing particles (China et al., 2013; Adachi and Buseck, 2013; Adachi et al., 2010). The common opinion based on TEM results is that bare rBC-containing particles adopt a fractal chain-like structure that will become more compact during the aging process (Wang et al., 2017). However, the representativeness of the TEM results remains a question. Since identifying rBC-containing particles using TEM is time-consuming work, the number of rBC-containing particles observed in one TEM study often ranges between hundreds and thousands, which is a tiny fraction of the ambient rBC-containing particles. Another way to determine the morphology of rBC-containing particles is to measure a physical index, such as the effective density ( $\rho_{\text{eff}}$ ), shape factor ( $\chi$ ), fractal dimension, etc. For instance, the  $\rho_{\text{eff}}$  is defined as the ratio of the

particle mass ( $M_p$ ) to the volume of its mobility equivalent sphere. The compactness of a particle can be determined by  
65 comparing the  $\rho_{\text{eff}}$  with the material density (the density of particles with a solid spherical structure). For particles with the  
same material density, a smaller  $\rho_{\text{eff}}$  indicates a looser structure.

In practice, a differential mobility analyzer (DMA), aerosol particle mass (APM) analyzer (or a centrifugal particle analyzer,  
CPMA) and condensation particle counter (CPC) are often integrated to obtain the  $M_p$  and mobility diameter ( $D_{\text{mob}}$ )  
simultaneously. Then, the  $\rho_{\text{eff}}$  is calculated by Eq. (1):

$$70 \quad \rho_{\text{eff}} = \frac{6M_p}{\pi D_{\text{mob}}^3} \quad (1)$$

The  $\rho_{\text{eff}}$  is often used in laboratory studies to determine the morphology of rBC (Xue et al., 2009;Pagels et al., 2009;Zhang et  
al., 2008). The freshly emitted rBC-containing particles are characterized by a significantly lower  $\rho_{\text{eff}}$  than the rBC material  
density of  $1.8 \text{ g/cm}^3$  suggested by (Bond et al., 2013). Zhang et al. (2008) observed that the  $\rho_{\text{eff}}$  of rBC-containing particles  
changed from  $0.56$  to  $1.60 \text{ g/cm}^3$  after  $\text{H}_2\text{SO}_4$  condensation, indicating reconstruction of rBC during the condensation process,  
75 which was consistent with the TEM results. Further studies showed that BC reconstruction was caused by the surface tension  
of the coating material, which differed for various coating compositions (Xue et al., 2009;Pagels et al., 2009).

In the laboratory, a high concentration of rBC-containing particles is normally generated by a laminar diffusion burner, and  
the  $\rho_{\text{eff}}$  of rBC-containing particles can be reasonably studied using the DMA-CPMA-CPC system. Investigation on the  $\rho_{\text{eff}}$  of  
rBC-containing particles using a DMA-CPMA-CPC tandem system would be difficult because there are substantial non-rBC  
80 particles in the ambient atmosphere. The  $\rho_{\text{eff}}$  determined using this approach is only representative of the characteristic of the  
bulk aerosols and not the rBC-containing particles. A single particle soot photometer (SP2) is able to distinguish rBC-  
containing particles from non-rBC particles at a single particle resolution. In this study, the CPC in the regular tandem DMA-  
CPMA-CPC system was replaced with the SP2, and the  $\rho_{\text{eff}}$  of the rBC-containing particles and the non-rBC particles were  
detected separately. Additionally, the key parameters related to the rBC mixing state, such as the mass of the rBC core, number  
85 fraction of rBC-containing particles and optical diameter of the rBC-containing particles, were well determined through SP2  
measurement. Thus, the mixing state and  $\rho_{\text{eff}}$  of rBC-containing particles were obtained simultaneously using the novel tandem  
DMA-CPMA-SP2 system.

In this study, field measurement using a tandem DMA-CPMA-SP2 system was performed from Dec. 20, 2018, to Jan. 04,  
2019, in the urban areas of Beijing to investigate the  $\rho_{\text{eff}}$  of ambient rBC-containing particles. The site is located in the tower  
90 campus of the State Key Laboratory of Atmospheric Boundary Layer Physics and Atmospheric Chemistry, Institute of  
Atmospheric Physics (LAPC, longitude:  $116.37^\circ\text{E}$ ; latitude:  $39.97^\circ\text{N}$ ). A more detailed description of the site can be found in  
the literature (Sun et al., 2016;Pan et al., 2019). Particles with different effective densities preselected by the DMA-CPMA  
were injected into the SP2. A comprehensive analysis was conducted with a focus on the relationship between the rBC-  
containing particle  $\rho_{\text{eff}}$  and the mixing state. To the best of our knowledge, this study is the first report of the  $\rho_{\text{eff}}$  of ambient  
95 rBC-containing particles. This study will help elucidate the microphysical properties of rBC-containing particles, which can  
reduce uncertainty in climate and health risk effect estimations.

## 2 Methods

### 2.1 Instruments

#### 2.1.1 Single particle soot photometer

100 The detailed principle of the SP2 (Droplet Measurement Technology, Inc., Boulder, CO, USA) has been reported in the literature (Shiraiwa et al., 2008; Moteki and Kondo, 2007). Briefly, due to the unique absorption ability of rBC, each single rBC-containing particle will absorb the high intensity laser (1064 nm, TEM00 mode) produced by the SP2. Then, the rBC is heated to the boiling point and emits incandescence. The peak incandescence intensity is nearly linearly correlated with the rBC mass. By detecting the incandescence, the rBC mass in each rBC-containing particle can be determined. The scattering  
105 signal of each particle is obtained simultaneously by the SP2. Particles that only have a scattering signal are identified as non-rBC particles, whereas particles with concurrence of incandescence and a scattering signal are identified as rBC-containing particles.

The SP2 was calibrated using Aquadag aerosols (lot 9627) and a polystyrene latex sphere (PSL, Nanosphere Size Standards, Duke Scientific Corp., USA) with sizes of 203 nm (lot 185856), 303 nm (lot 189903), and 400 nm (lot 189904). Because the  
110 SP2 is more sensitive to Aquadag than ambient rBC (Laborde et al., 2013), the incandescent signal was corrected by scaling a factor of 0.75 in the ambient measurement. The total uncertainty of the rBC mass measured by the SP2 was estimated to be 30%.

#### 2.2 Tandem system

The tandem system in this study included a DMA (model 3085A, TSI Inc., USA), CPMA (Cambustion Ltd.), condensation  
115 particle counter (CPC, model 3775, TSI Inc., USA) and SP2. A schematic diagram of the measurement system is provided in Fig. S1.

The CPMA was used to select particles with a known mass based on a specific charge-to-mass ratio by imposing opposite centrifugal and electric forces on the charged aerosols inside (Olfert and Collings, 2005). The DMA was used to select particles with a known mobility diameter ( $D_{mob}$ ) based on the particles' electromobility. The tandem DMA-CPMA system was capable  
120 of selecting particles with a known  $\rho_{eff}$ . The reliability of the DMA-CPMA tandem system was tested using PSL particles ( $\rho_{eff}$ : 1.05 g/cm<sup>3</sup>). In general, the tandem system overestimated the  $\rho_{eff}$  by 5% with a mode  $\rho_{eff}$  value of 1.10 g/cm<sup>3</sup>, as shown in Fig. S2. The multiple charged influences (Fig. S2) were negligible.

Particles with known effective densities preselected by the DMA-CPMA system were injected into the SP2 to obtain information on the corresponding rBC. In practice, the mobility diameter selected by the DMA was set at a constant value of  
125 240 nm. The setpoints of the CPMA were 5.79, 7.24, 8.69, 10.13, 11.58, and 13.03 fg, which corresponded to a  $\rho_{eff}$  of 0.8, 1.0, 1.2, 1.4, 1.6, and 1.8 g/cm<sup>3</sup>, respectively. Each CPMA setpoint was held for 10 min, and the duration of a whole scan turn of the six setpoints was 1 hour. In this study, the sum of particle numbers over ten minutes was used to present the temporal variation of particles with different  $\rho_{eff}$  values.

## 2.3 Data analysis

### 130 2.3.1 Determination of the bulk effective density

The number concentration of particles with six different target  $\rho_{\text{eff}}$  values were measured consecutively on 10-minutes basis. Thus, a distribution of different effective densities could be obtained every hour. Previous studies (Qiao et al., 2018; Momenimovahed and Olfert, 2015) often used a log-normal or Gaussian function to fit the  $\rho_{\text{eff}}$  distribution. The  $\rho_{\text{eff}}$  of the bulk aerosols was determined to be the peak location of the fit function. Due to the limited  $\rho_{\text{eff}}$  measurement points in this study, the bulk aerosol density was calculated using a simple method as shown in Eq. 2.  $\rho_i$  denotes the  $\rho_{\text{eff}}$  with the maximum particle number in one hour, and  $N_i$  denotes the number of particles with  $\rho_i$ .  $\rho_{i-1}$  and  $\rho_{i+1}$  denote the adjacent effective density set points of  $\rho_i$ .

$$\rho_{\text{bulk}} = \frac{\rho_i * N_i + \rho_{i-1} * N_{i-1} + \rho_{i+1} * N_{i+1}}{N_i + N_{i-1} + N_{i+1}} \quad (2)$$

We tested this method to calculate the  $\rho_{\text{eff}}$  of PSL, as shown in Fig. S3. The  $\rho_{\text{eff}}$  determined using this approach was 1.09 g/cm<sup>3</sup>, which was very close to the given density of 1.05 g/cm<sup>3</sup>.

### 2.3.2 Determination of the optical diameter

For non-rBC particles, the scattering cross-sections are proportional to the peak scattering intensity measured by the SP2. The optical diameter ( $D_{\text{opt}}$ ) was calculated through the Mie theory with a refractive index of 1.48 and assumption of a spherical structure. Since rBC-containing particles evaporate in the laser beam, leading to a decrease in the scattering cross-section, a leading edge only (LEO) fit (Gao et al., 2007; Liu et al., 2014; Pan et al., 2017) method was used to retrieve the undisturbed peak scattering intensity. By assuming a core-shell structure and using the refractive indices determine by (Taylor et al., 2015), 1.48 for coating and 2.26-1.26i for rBC core, the  $D_{\text{opt}}$  of the rBC-containing particles can also be calculated based on the Mie-scattering theory.

### 2.3.3 Determination of the shape factor and void fraction

The shape factor  $\chi$  is an applicable parameter describing irregularity of a particle. When  $\chi$  is equal to 1, the particle is in a regular spherical structure, whereas a larger  $\chi$  indicates that the particle is more irregular. The  $\chi$  of the rBC-containing particles was calculated using the following equation (Zhang et al., 2016) in this study:

$$\chi = \frac{D_{\text{mob}} \times C_c(D_{\text{mev}})}{D_{\text{mev}} \times C_c(D_{\text{mob}})} \quad (3)$$

where  $D_{\text{mob}}$  is the mobility diameter,  $D_{\text{mev}}$  is the mass equivalent diameter, and  $C_c$  is the Cunningham slip correction factor (Decarlo et al., 2004).

The void volume ratio ( $R_{\text{void}}$ ) was also used to represent the compactness of rBC-containing particles in this study. The  $R_{\text{void}}$  is 0 for particles with an ideal solid spherical and increases when the structure loosens. The  $R_{\text{void}}$  is calculated by Eq (4):

$$R_{\text{void}} = 1 - \frac{D_{\text{me}}^3}{D_{\text{m}}^3} \quad (4)$$

### 2.3.4 Determination of the coating thickness

160 The mass ratio ( $M_R$ ) of coating to rBC core was used to represent the coating thickness in this study. The mass of the rBC-containing particle ( $M_p$ ) was directly measured by CPMA and the mass of rBC core ( $M_{rBC}$ ) was measured by SP2. Then, the  $M_R$  was calculated by Eq (5):

$$M_R = \frac{M_p - M_{rBC}}{M_{rBC}} \quad (5)$$

165 The uncertainty of  $M_R$  was determined to be 31.6% and the uncertainties of the major parameters using in this paper can be found in supplementary.

## 3 Results

### 3.1 Constraining factors of effective density

The temporal variation in the number concentrations of rBC-containing and non-rBC particles and the mass concentration of non-refractory  $PM_{2.5}$  (NR- $PM_{2.5}$ ) measured by a time-of-flight aerosol chemical speciation monitor (ToF-ACSM) are shown in Fig. 1. Four pollution events and one lasting clean episode were observed during the observation period and were denoted EP 1-5. EP 3 was defined as the clean episode with a  $PM_{2.5}$  mass concentration less than  $10 \mu\text{g}/\text{cm}^3$ . The  $PM_{2.5}$  mass concentration was higher than  $50 \mu\text{g}/\text{cm}^3$  during the other four pollution episodes. The backward trajectories of the five episodes are illustrated in Fig. S4. Beijing was majorly affected by the local air mass or southern polluted air mass during the pollution episodes. In contrast, the clean northwest air mass dominated in Beijing during the clean episode.

175 For simplicity, the effective densities of non-rBC and rBC-containing particles were called  $\rho_{\text{non-rBC}}$  and  $\rho_{\text{rBC}}$  separately. Whereas the effective density of bulk non-rBC and rBC-containing particles calculated by equation (2) was called  $\rho_{\text{non-rBC,bulk}}$  and  $\rho_{\text{rBC,bulk}}$ . The bulk effective density reflects the number distribution of particles with different effective densities. For example, the number fractions of non-rBC particles with lower  $\rho_{\text{non-rBC}}$  ( $0.8\text{-}1.2 \text{ g}/\text{cm}^3$ ) were  $\sim 70\%$  during EP 2 and EP 4 and this value was significantly lower ( $\sim 20\%$ ) during EP 1 and EP 5. Correspondingly, the  $\rho_{\text{non-rBC,bulk}}$  was calculated to be  $1.18$  and  $1.20 \text{ g}/\text{cm}^3$  in EP 2 and EP 4 lower than  $1.43$  and  $1.40 \text{ g}/\text{cm}^3$  in EP 1 and EP 5. The variation in  $\rho_{\text{non-rBC}}$  was mainly caused by different non-rBC compositions in different cases, since the  $\rho_{\text{eff}}$  of different compositions varies. The  $\rho_{\text{eff}}$  value of  $(\text{NH}_4)_2\text{SO}_4$  and  $\text{NH}_4\text{NO}_3$  particles was  $1.75 \text{ g}/\text{cm}^3$  (Qiao et al., 2018), whereas those of organics depended on their compositions and usually were between  $0.64$  and  $1.49 \text{ g}/\text{cm}^3$  (Malloy et al., 2009; Hallquist et al., 2009; Bahreini et al., 2005; Turpin and Lim, 2001). Turpin and Lim (2001) suggested an overall  $\rho_{\text{eff}}$  of  $1.2 \text{ g}/\text{cm}^3$  for organic aerosols in Los Angeles, and Hallquist et al. (2009) recommended a  $\rho_{\text{eff}}$  of  $1.4 \text{ g}/\text{cm}^3$  for secondary organic aerosols in the absence of direct measurement. In general, the  $\rho_{\text{eff}}$  values of organics are always lower than those of inorganic compounds. The lower  $\rho_{\text{non-rBC}}$  may indicate a higher mass fraction of organic compounds in the non-rBC particles. In fact, although the composition may slightly differ between NR- $PM_{2.5}$  and particles with  $D_{\text{mob}}=240 \text{ nm}$  as observed in this study, the higher organic fractions in NR- $PM_{2.5}$  in EP 2 and EP 4 (66% and 59%) may indicate an organic dominant pollution environment and thus a higher organic fraction in particles with  $D_{\text{mob}}=240$

190 nm consistent with the lower  $\rho_{\text{non-rBC,bulk}}$  in these two episodes. Furthermore, the relationship between effective density and organic fraction was assessed throughout the observation period, as shown in Fig. S5. The  $\rho_{\text{non-rBC,bulk}}$  value was apparently low in the high organic fraction environment during the whole observation period. The  $\rho_{\text{rBC,bulk}}$  was also lower in the more organic fraction condition similar to that of the non-rBC particles, which was mostly due to composition of coating matters. In this study we presumed that, first, a lower  $\rho_{\text{non-rBC,bulk}}$  value means a higher organic fraction in the non-rBC particles. Second, composition of non-rBC particles and the coatings of rBC-containing particles were similar.

To better understand the morphological impacts on  $\rho_{\text{eff}}$ , the optical diameters ( $D_{\text{opt}}$ ) of non-rBC and rBC-containing particles were compared to that of  $D_{\text{mob}}$ , as shown in Fig. 2. The particle shapes are spherical if  $D_{\text{mob}}$  is the same as  $D_{\text{opt}}$ , since the structure is assumed to be spherical in the  $D_{\text{opt}}$  calculation through Mie-theory. For non-rBC particles with a  $\rho_{\text{non-rBC}}$  larger than 1.4 g/cm<sup>3</sup>,  $D_{\text{mob}}$  and  $D_{\text{opt}}$  are nearly the same. For non-rBC particles with a  $\rho_{\text{non-rBC}} = 1.0$  or 1.2 g/cm<sup>3</sup>, the  $D_{\text{opt}}$  is slightly lower than the  $D_{\text{mob}}$ . The refractive indices for (NH<sub>4</sub>)<sub>2</sub>SO<sub>4</sub>, NaCl and secondary organic aerosols have been determined to be 1.51, 1.53 and 1.44-1.5, respectively (Nakayama et al., 2010; Schnaiter et al., 2003; Toon et al., 1976). An even lower refractive index (1.42) was found for ambient non-rBC particles (Zhang et al., 2018). The constant refractive index of 1.48 may underestimate the  $D_{\text{opt}}$  of non-rBC particles with lower  $\rho_{\text{non-rBC}}$ , since the refractive indices of organic aerosols may be lower than those of inorganics. Different refractive index assumptions were used to calculate the  $D_{\text{opt}}$ , as denoted by the red and blue dashed lines in Fig. 2. When the variation in the refractive indices was taken into account, the  $D_{\text{opt}}$  was considered to be the same as the  $D_{\text{mob}}$  for non-rBC particles with a  $\rho_{\text{non-rBC}} = 1.0$  or 1.2 g/cm<sup>3</sup>. For non-rBC particles with a  $\rho_{\text{non-rBC}}$  of 0.8 g/cm<sup>3</sup>, the lower  $D_{\text{opt}}$  may be caused by the lower refractive indices for some specific compounds or the non-spherical morphology. However, the fraction of this non-rBC was negligible, as shown in Fig. 1. Thus, the non-rBC particles mostly adopted a spherical structure. The mean  $D_{\text{opt}}$  was 179, 197, and 214 nm for rBC-containing particles with a  $\rho_{\text{rBC}} = 0.8, 1.0, \text{ and } 1.2 \text{ g/cm}^3$ , respectively, which were significantly lower than the  $D_{\text{mob}}$  values. This decrease could not be explained by variation in the refractive indices, as shown in Fig. 2(b), indicating that the morphologies of these rBC-containing particles were not spherical. The  $D_{\text{opt}}$  was the same as the  $D_{\text{mob}}$  when the  $\rho_{\text{rBC}}$  was equal to 1.6 or 1.8 g/cm<sup>3</sup>, suggesting that the particles approximate to spherical structure. rBC-containing particles with a  $\rho_{\text{rBC}} = 1.4 \text{ g/cm}^3$  were placed at the morphological transition point. The differences between the 75th and 25th percentiles of the  $D_{\text{opt}}$  were larger for the rBC-containing particles than for the non-rBC particles, as denoted by the box length. This larger difference may be caused by the complex morphology of rBC-containing particles compared to that of non-rBC particles. In general, the non-rBC particles mostly had a spherical structure, and the  $\rho_{\text{non-rBC}}$  was majorly influenced by the composition. A lower fraction of organics contributed to the increase in the  $\rho_{\text{non-rBC}}$ . The  $\rho_{\text{rBC}}$  was controlled by the combined effect of the morphology and coating composition. A fractal structure and a more organic coating tend to decrease the  $\rho_{\text{rBC}}$ .

### 220 3.2 The relationship between the morphology and effective density of rBC-containing particles

Figure 3 depicts the variations of the  $\chi$  and  $R_{\text{void}}$  values as a function of  $\rho_{\text{rBC}}$ .  $\chi$  is a physical index representing the regularity of a particle; the theoretical  $\chi$  for a spherical particle is 1 regardless of the void inside, and a larger  $\chi$  means a more irregular

particle (Decarlo et al., 2004). In practice, the  $\chi$  of rBC-containing particles ranges from 1-4 (Table 2) mostly due to the combustion material, combustion temperature, aging degree, etc. The largest  $\chi$  (1.4) observed in this study was lower than that of freshly emitted rBC-containing particles from a diesel truck ( $\chi=2.1$ ), methane flame ( $\chi=1.87$ ) and propane flame ( $\chi=4.0$ ) and was in the range ( $\chi=1-2.8$ ) of rBC-containing particles with different aging degrees (Qiu et al., 2014;Peng et al., 2016). Zhang et al. (2016) suggested that the  $\rho_{\text{rBC}}$  of thinly coated rBC-containing particles was  $0.3 \text{ g/cm}^3$ . Direct measurements of vehicle exhaust always obtain a  $\rho_{\text{rBC}}$  of  $0.3-0.5 \text{ g/cm}^3$  (Momenimovahed and Olfert, 2015). Because the lower detection limit of  $\rho_{\text{rBC}}$  was set to  $0.8 \text{ g/cm}^3$ , fresh rBC-containing particles might not have been observed in this study. Indeed, the rBC-containing particles observed in this study were actually aged rBC-containing particles with moderate irregularity.

The  $\chi$  values showed a decreasing trend with the increasing  $\rho_{\text{rBC}}$ , indicating a more regular shape for rBC-containing particles with a larger  $\rho_{\text{rBC}}$ , which was consistent with previous studies (Qiu et al., 2014;Peng et al., 2016). When the  $\rho_{\text{rBC}}$  is less than  $1.4 \text{ g/cm}^3$ , the  $\chi$  decreases significantly with the increase in  $\rho_{\text{rBC}}$ . However,  $\chi$  varies slowly between 1 and 1.1 when the  $\rho_{\text{rBC}}$  is larger than  $1.4 \text{ g/cm}^3$ . A similar variation trend was also found for  $R_{\text{void}}$ .  $R_{\text{void}}$  decreases significantly from 0.5 to 0.1 and varies slowly between 0.1 and 0 when the  $\rho_{\text{rBC}}$  is larger than  $1.4 \text{ g/cm}^3$ . These results are similar to those from the comparison between  $D_{\text{opt}}$  and  $D_{\text{mob}}$ ; the morphology of rBC-containing particles changed from an irregular and loose structure to a compact spherical structure with the increasing  $\rho_{\text{rBC}}$ . Thus, a  $\rho_{\text{rBC}}$  of  $1.4 \text{ g/cm}^3$  may be the morphological transition point in this study. Using a smog chamber, Peng et al. (2016) also observed a change in the  $\rho_{\text{rBC}}$  from  $\sim 0.5 \text{ g/cm}^3$  to  $1.4 \text{ g/cm}^3$  during the aging process and found that rBC-containing particles with a  $\rho_{\text{rBC}} = 1.4 \text{ g/cm}^3$  had a  $\chi \sim 1$ .

We found that rBC-containing particle had a larger  $\chi$  value and  $R_{\text{void}}$  at the condition when  $\rho_{\text{non-rBC,bulk}}$  is smaller, especially for irregular particles (Fig. 3a). It may imply that different coating composition played a different role in the morphology reconstructing of rBC-containing because  $\rho_{\text{non-rBC,bulk}}$  reflected the composition of non-rBC which may relate to the coating composition of rBC in some degree (Fig. S6). The rBC-containing particles could reach a compact spherical structure when the  $\rho_{\text{rBC}}$  was  $1.2 \text{ g/cm}^3$  with an  $\chi$  of 1.05 and a  $R_{\text{void}}$  of 0.08 when  $1.1 \text{ g/cm}^3 < \rho_{\text{non-rBC,bulk}} < 1.3 \text{ g/cm}^3$ , whereas the morphological transition of  $\rho_{\text{rBC}}$  was higher for rBC-containing particles at a higher  $\rho_{\text{non-rBC,bulk}}$  condition.

### 3.3 Mass ratio of coatings to the rBC core of rBC-containing particles with different $\rho_{\text{eff}}$ values

The mass ratio ( $M_{\text{R}}$ ) of the coating to the rBC core is used to represent the coating thickness in this study. The coating thickness is an index of the aging degree of rBC-containing particles since condensation and coagulation will lead to an increase in the coating thickness during the aging process. As shown in Fig. 4, rBC-containing particles with larger  $\rho_{\text{rBC}}$  values had more coating. This phenomenon explains the morphological change that occurs with an increasing  $\rho_{\text{rBC}}$ . The surface tension imposed by the coating was found to shrink the rBC core (Zhang et al., 2016). After coating, rBC-containing particles with larger hygroscopicity more easily obtain surface water, which enlarges the surface tension and shrinks the rBC-containing particles to a more compact structure (Zhang et al., 2008). Moreover, the coatings are able to fill the void of rBC-containing particles, resulting in a more compact structure (Pagels et al., 2009). Thus, increasing the coating makes rBC-containing particles more compact, and the compact structure leads to a larger effective density, as observed.

Recently, studies using different methods have proven the occurrence of morphological change of rBC-containing particles with an increase in the coating thickness. Peng et al. (2016) observed that rBC-containing particles changed to a compact spherical structure when the ratio of the coating thickness to the rBC core diameter reached 0.8-1, corresponding to a  $M_R$  of 4.5-6.5. By comparing the measured and modeled scattering cross-sections of rBC-containing particles, Liu et al. (2017) found that the measured scattering cross-section agreed well with the core-shell model prediction when the  $M_R$  was larger than 3, suggesting adoption of a spherical morphology by rBC-containing particles with a large  $M_R$ . The morphology of rBC-containing particles seems to change to be spherical at a certain  $M_R$  point. In this study, the  $M_R$  was nearly invariant and fluctuated between 6 and 8 when the  $\rho_{\text{eff}}$  was larger than  $1.4 \text{ g/cm}^3$ , suggesting that the rBC-containing particles were mostly spherical in structure when the  $M_R$  was larger than 6-8.

In the real atmosphere, the variant temperature and relative humidity may also contribute to the morphological variation of rBC-containing particles, which makes the morphological transition  $M_R$  point more complicated and thus different from that reported in previous studies. However, an agreement has been reached concerning the mechanism by which the morphology changes with the increasing coating thickness. A  $M_R$  of 7 was determined to be the morphological transition point in Beijing in winter. The morphological transition  $M_R$  or volume ratio may be very useful for parameterization in atmospheric models.

Thus, more observations are needed to explore the variation and constraining factors of the morphological transition  $M_R$ . Previous studies have always used a shell/core ratio (S/C) to represent the coating thickness. The  $M_R$  of rBC-containing particles with a  $\rho_{\text{rBC}}=0.8 \text{ g/cm}^3$  averaged 2.0, corresponding to an S/C of 1.5, and the  $M_R$  of rBC-containing particles with a  $\rho_{\text{rBC}}=1.4 \text{ g/cm}^3$  averaged 7.0, corresponding to an S/C of 2.15. Typically, the S/C ratio of freshly emitted BC observed at urban sites was lower than 1.2 (Liu et al., 2014; Laborde et al., 2013). In this study, rBC-containing particles with a  $\rho_{\text{rBC}}$  of  $0.8 \text{ g/cm}^3$  were characterized as having an irregular and loose structure with  $\chi = 1.4$  and  $R_{\text{void}}=0.5$ . Since the  $\rho_{\text{rBC}}$  increased with the increase in the  $M_R$  or S/C, the observed average S/C = 1.2 at the urban site suggested that most rBC-containing particles in the urban site might have a  $\rho_{\text{rBC}}$  lower than  $0.8 \text{ g/cm}^3$  and thus a more irregular structure.

### 3.4 The morphology of bulk rBC-containing particles

The number distributions of  $\rho_{\text{rBC}}$  and  $\rho_{\text{non-rBC}}$  were counted to evaluate the morphological characteristics of the bulk rBC-containing particles in the ambient environment, as shown in Fig. 5. Generally, the  $\rho_{\text{rBC}}$  and  $\rho_{\text{non-rBC}}$  number distributions exhibited a unimodal distribution except for the  $\rho_{\text{rBC}}$  distribution in EP 3 (the clean period). Observations of rBC-containing particles indicated that the coating thickness distribution always exhibited a clear bimodal pattern (Liu et al., 2014; Wu et al., 2017). rBC-containing particles were observed with a thin coating, which was mostly attributed to local traffic emissions, and with a thick coating, which might be the result of biomass emissions or the aging process. The aged rBC-containing particles with a  $\rho_{\text{rBC}} > 0.8 \text{ g/cm}^3$  observed in this study may exactly correspond to the rBC-containing particles with a thick coating and thus exhibit a unimodal pattern. We speculate that the  $\rho_{\text{rBC}}$  number distribution will exhibit a bimodal pattern if the detection limit is sufficiently low and the left peak in the expected bimodal pattern corresponds to the rBC-containing particles with thin

coatings. The  $\rho_{\text{rBC}}$  distribution in EP 3 may be influenced by the thinly-coated rBC-containing particles, which might be present  
290 in relatively higher numbers during the clean period.

The  $\rho_{\text{rBC,bulk}}$  and  $\rho_{\text{non-rBC,bulk}}$  were separately estimated to be 1.21 g/cm<sup>3</sup> and 1.39 g/cm<sup>3</sup>, respectively, throughout the observation  
period. Notably, due to the detection limit, the  $\rho_{\text{rBC,bulk}}$  in this study was determined for aged rBC-containing particles, and the  
true  $\rho_{\text{rBC,bulk}}$  was expected to be lower if fresh rBC-containing particles were taken into consideration. However, even for these  
aged rBC-containing particles, the morphology was mostly in a fractal structure, because the  $\rho_{\text{rBC,bulk}}$  (1.21 g/cm<sup>3</sup>) was smaller  
295 than the morphological transition  $\rho_{\text{rBC}}$  (1.40 g/cm<sup>3</sup>). Wang et al. (2017) proved that only 12% of rBC-containing particles were  
in an embedded structure and that 88% of rBC-containing particles were in a bare or partly coated structure in urban sites  
through direct TEM observation. Our results provided evidence for the irregularity of rBC-containing particles based on  
assessment of more particle numbers.

The  $\rho_{\text{eff}}$  was separately counted in the five episodes, as shown in Fig. 5, to investigate variation in  $\rho_{\text{eff}}$  under different pollution  
300 situations. The  $\rho_{\text{rBC,bulk}}$  was 1.37, 1.01, 1.15, 1.01, and 1.21 g/cm<sup>3</sup> during EP 1-5, and the corresponding  $\rho_{\text{non-rBC,bulk}}$  was 1.43,  
1.18, 1.40, 1.20, and 1.40 g/cm<sup>3</sup>, respectively. According to Fig. 3a, the morphological transition  $\rho_{\text{rBC}}$  points were 1.2 g/cm<sup>3</sup> in  
EP 2 and EP 4 and 1.4 g/cm<sup>3</sup> in EP 1, EP 3, and EP 5 due to the different  $\rho_{\text{non-rBC,bulk}}$  value. The  $\rho_{\text{rBC,bulk}}$  in the five episodes  
was lower than that of the morphological transition  $\rho_{\text{rBC}}$  regardless of the pollution conditions, indicating that a substantial  
number of rBC-containing particles were in a fractal structure even under pollution conditions. However, the  $\rho_{\text{rBC,bulk}}$  in EP3  
305 was smaller than that in EP1 and EP5, which might suggest a more compact structure of rBC-containing particles in pollution  
conditions, since the morphological transition  $\rho_{\text{rBC}}$  was similar during these three episodes.

The number fraction of rBC-containing particles in the total measured particles (rBC-containing and non-rBC particles)  
increased with the decrease in the  $\rho_{\text{eff}}$ , as shown in Fig. 6. rBC-containing particles only accounted for 10-20% of particles  
with a  $\rho_{\text{eff}} = 1.6$  g/cm<sup>3</sup>, whereas this fraction significantly increased to ~60% for particles with a  $\rho_{\text{eff}} = 0.8$  g/cm<sup>3</sup>. The data from  
310 the five episodes all followed the same tendency, and the maximum number fraction of rBC-containing particles was reached  
when the  $\rho_{\text{eff}}$  was equal to 0.8 g/cm<sup>3</sup>. A power function was used to fit the data and showed that the number fraction of rBC  
would be 100% if the  $\rho_{\text{eff}}$  was less than 0.73 g/cm<sup>3</sup>. Rissler et al. (2014) observed a bimodal  $\rho_{\text{eff}}$  distribution of ambient aerosols.  
The  $\rho_{\text{eff}}$  of aerosols in the two peaks ranged separately from 0.30 - 0.80 g/cm<sup>3</sup> and 1.28 - 1.46 g/cm<sup>3</sup>. The mass of aerosols  
with a  $\rho_{\text{eff}}$  of 0.30 - 0.80 g/cm<sup>3</sup> only lost 10% after being heated to 300 °C, indicating that most of these particles were fresh  
315 rBC-containing particles, which was consistent with our inference. Thus, if the measurement site was located in an area with  
enough fresh BC emission, the bimodal  $\rho_{\text{eff}}$  distribution of ambient aerosols was often observed (Qiao et al., 2018; Liu et al.,  
2015; Rissler et al., 2014), since the  $\rho_{\text{eff}}$  of fresh rBC-containing particles was sufficiently small with no disturbance by non-  
rBC particles. However, as shown in Fig. 6, the  $\rho_{\text{eff}}$  distributions of non-rBC and aged rBC-containing particles overlapped  
and could not be distinguished through a simple DMA-APM/CPMA-CPC system. Our study suggested that the second peak  
320 often observed in previous  $\rho_{\text{eff}}$  measurements was actually a mixture of non-rBC and aged rBC-containing particles. Rissler et  
al. (2014) used “dense” particles to describe particles with a  $\rho_{\text{eff}}$  of 1.28 - 1.46 g/cm<sup>3</sup>. This expression might be not very  
accurate, since nearly 10-40% of the particles were aged rBC-containing particles with a fractal structure ( $\chi=1-1.2$ ).

### 3.5 Optical properties of rBC-containing particles with different $\rho_{\text{eff}}$

Since the morphology of rBC-containing particles was mostly in a fractal structure as discussed above, the simple core-shell structure treatment in the atmospheric model might cause bias in the optical property estimate of rBC-containing particles. An aggregate model was established, and the optical properties were calculated by solving Maxwell's equation based on the superposition T-matrix method (Wu et al., 2018). As shown in Fig. 7(a), large discrepancies in the scattering cross-sections ( $\sigma_{\text{SC}}$ ) between the core-shell model and measurement were found in the small  $\rho_{\text{rBC}}$  range, indicating the strong impact of morphology on optical properties. An aggregate model can better capture the  $\sigma_{\text{SC}}$  characteristics than a perfect shell-core model when the  $\rho_{\text{rBC}}$  is smaller than 1.4 g/cm<sup>3</sup>. When the  $\rho_{\text{rBC}}$  is 0.8 g/cm<sup>3</sup>, the  $\sigma_{\text{SC}}$  predicted by the aggregate model with an rBC core fractal dimension ( $D_f$ ) of 2.0-2.2 agrees well with the measurement. With an increase in the  $\rho_{\text{rBC}}$ , the measured  $\sigma_{\text{SC}}$  is consistent with the predicted value from the aggregate model obtained using the larger rBC core fractal dimension. This result may imply that the rBC core becomes more compact and regular with an increase in the  $\rho_{\text{rBC}}$  or coating thickness consistent with the laboratory results (Pagels et al., 2009; Xue et al., 2009).

Figure 7(b) exhibits the estimated mass absorption cross-sections (MACs) from different models. The overestimation of the MAC using the core-shell structure averaged 16.7% compared to that of the aggregate model when the  $\rho_{\text{rBC}}$  was less than 1.4 g/cm<sup>3</sup>. Additionally, the measured  $\sigma_{\text{SC}}$  with a  $\rho_{\text{rBC}} = 1.6$  g/cm<sup>3</sup> was similar to the predicted values of models 1 and 2, indicating a near spherical structure of the rBC-containing particles. However, the MAC predicted by models 1 and 2 varied. Although laboratory studies proved that the rBC core shrank after coating, an irregular rBC core was often observed even in thickly-coated cases in the ambient measurement (Adachi et al., 2010; Zhang et al., 2016), suggesting that model 2 might be closer to the realistic thickly-coated situation. Since model 1 overestimated the MAC by 7.4% with a  $\rho_{\text{rBC}} = 1.6$  g/cm<sup>3</sup> compared to that of model 2, the morphology of the rBC core should also be considered, even in cases with a large  $\rho_{\text{rBC}}$  or thickly-coated condition. In general, the commonly observed light absorption enhancement in pollution conditions cannot simply be attributed to the "lensing effect". The morphological change of rBC-containing particles and the BC core may also play an important role in light absorption enhancement.

### 4 Conclusion

A novel tandem DMA-CPMA-SP2 system was used to investigate the effective density of rBC-containing particles ( $\rho_{\text{rBC}}$ ) and their relationship with the rBC mixing state in Beijing. Aerosols with the same mobility diameter (240 nm) and different  $\rho_{\text{eff}}$  values (0.8, 1.0, 1.2, 1.4, 1.6, and 1.8 g/cm<sup>3</sup>) were preselected by the DMA-CPMA system and injected into the SP2 to obtain the corresponding mixing state. The results showed that the  $\rho_{\text{rBC}}$  could reflect the morphology of rBC-containing particles. The dynamic shape factor of rBC-containing particles decreased from 1.4 to 1 with the increase in the  $\rho_{\text{rBC}}$ , indicating that the morphology of the rBC-containing particles changed from an irregular loose structure to a compact spherical structure. rBC-containing particles with  $\rho_{\text{rBC}}$  values of 0.8, 1.0, and 1.2 g/cm<sup>3</sup> mostly adopted a non-spherical structure, whereas those with  $\rho_{\text{rBC}}$  values of 1.6 and 1.8 g/cm<sup>3</sup> were in a spherical structure. The  $\rho_{\text{rBC}} = 1.4$  g/cm<sup>3</sup> was determined to be the morphological

355 transition point in this study. The mass ratio ( $M_R$ ) of the coatings to the rBC core was calculated for rBC-containing particles with different  $\rho_{\text{rBC}}$  values. The  $M_R$  gradually increased from 2 to 6-8 with the increase in the  $\rho_{\text{rBC}}$  when that latter measure was less than  $1.4 \text{ g/cm}^3$  and stayed invariant when the  $\rho_{\text{rBC}}$  was larger than  $1.4 \text{ g/cm}^3$ , suggesting that the increased coating thickness during the aging process was the cause of morphological changes and that the rBC-containing particles tended to be spherical when the  $M_R$  was larger than 6-8 in the winter in Beijing.

360 The morphological characteristics of the bulk ambient rBC-containing particles were investigated by calculating the bulk effective density of rBC-containing particles ( $\rho_{\text{rBC,bulk}}$ ) considering the number distribution of  $\rho_{\text{rBC}}$ . The  $\rho_{\text{rBC,bulk}}$  averaged  $1.21 \text{ g/cm}^3$  during the whole observation period and was lower than the morphological transition  $\rho_{\text{rBC}}$  regardless of the pollution conditions. The  $\rho_{\text{rBC,bulk}}$  was overestimated due to the lower detection limit in this study (set to  $0.8 \text{ g/cm}^3$ ), which was larger than the  $\rho_{\text{rBC}}$  of freshly emitted rBC-containing particles. However, the  $\rho_{\text{rBC,bulk}}$  was still lower than the morphological transition

365  $\rho_{\text{rBC}}$ , suggesting that the rBC-containing particles were mostly not in a core-shell structure in the ambient condition. An aggregate model considering the morphological information of rBC-containing particles was approved to better represent and to evaluate the optical properties of rBC-containing particles. Generally, the core-shell model overestimated light absorption compared to that of the aggregate model by 16.7% for rBC-containing particles with a  $\rho_{\text{rBC}}=0.8-1.4 \text{ g/cm}^3$ . This study revealed that a substantial number of rBC-containing particles were in an irregular structure in the ambient atmosphere and highlighted

370 the importance of morphology for optical property estimates. A proper parameterization considering rBC-containing particle morphological changes with  $M_R$  and a morphology-dependent optical model may help reduce the uncertainty in atmospheric modeling.

### Data availability

375 To request the data given in this study, please contact Dr. Xiaole Pan at the Institute of Atmospheric Physics, Chinese Academy of Sciences, via email ([panxiaole@mail.iap.ac.cn](mailto:panxiaole@mail.iap.ac.cn)).

### Author contributions

H.L, X.P designed the research; Y.W, H.L performed the optical simulation using T-matrix method. H.L, X.P, D.W, X.L, Y.T, Y.S, P.F, Z.W performed experiments; H.L, X.P, Y.T performed the data analysis; H.L, X.P wrote the paper.

380

### Acknowledgements

This study was supported by the National Natural Science Foundation of China (No. 41605104).

## Reference

- 385 Adachi, K., Chung, S. H., and Buseck, P. R.: Shapes of soot aerosol particles and implications for their effects on climate, *J. Geophys. Res.-Atmos.*, 115, Artn D15206  
10.1029/2009jd012868, 2010.  
Adachi, K., and Buseck, P. R.: Changes of ns-soot mixing states and shapes in an urban area during CalNex, *J. Geophys. Res.-Atmos.*, 118, 3723-3730, 10.1002/jgrd.50321, 2013.
- 390 Alfoldy, B., Giechaskiel, B., Hofmann, W., and Drossinos, Y.: Size-distribution dependent lung deposition of diesel exhaust particles, *J Aerosol Sci*, 40, 652-663, 10.1016/j.jaerosci.2009.04.009, 2009.  
Apte, J. S., Marshall, J. D., Cohen, A. J., and Brauer, M.: Addressing Global Mortality from Ambient PM<sub>2.5</sub>, *Environ Sci Technol*, 49, 8057-8066, 10.1021/acs.est.5b01236, 2015.  
Bahreini, R., Keywood, M. D., Ng, N. L., Varutbangkul, V., Gao, S., Flagan, R. C., Seinfeld, J. H., Worsnop, D. R., and Jimenez, J. L.: Measurements of secondary organic aerosol from oxidation of cycloalkenes, terpenes, and m-xylene using an Aerodyne aerosol mass spectrometer, *Environ Sci Technol*, 39, 5674-5688, 10.1021/es048061a, 2005.
- 395 Bond, T. C., Doherty, S. J., Fahey, D., Forster, P., Berntsen, T., DeAngelo, B., Flanner, M., Ghan, S., Kärcher, B., and Koch, D.: Bounding the role of black carbon in the climate system: A scientific assessment, *Journal of Geophysical Research: Atmospheres*, 118, 5380-5552, 2013.
- 400 Cappa, C. D., Onasch, T. B., Massoli, P., Worsnop, D. R., Bates, T. S., Cross, E. S., Davidovits, P., Hakala, J., Hayden, K. L., Jobson, B. T., Kolesar, K. R., Lack, D. A., Lerner, B. M., Li, S. M., Mellon, D., Nuaaman, I., Olfert, J. S., Petaja, T., Quinn, P. K., Song, C., Subramanian, R., Williams, E. J., and Zaveri, R. A.: Radiative Absorption Enhancements Due to the Mixing State of Atmospheric Black Carbon, *Science*, 337, 1078-1081, 10.1126/science.1223447, 2012.  
China, S., Mazzoleni, C., Gorkowski, K., Aiken, A. C., and Dubey, M. K.: Morphology and mixing state of individual freshly emitted wildfire carbonaceous particles, *Nat Commun*, 4, ARTN 2122  
10.1038/ncomms3122, 2013.
- 405 Decarlo, P., Slowik, J., Worsnop, D., PaulDavidovits, and Jimenez, J.: Particle Morphology and Density Characterization by Combined Mobility and Aerodynamic Diameter Measurements. Part 1: Theory, *Aerosol Science & Technology*, 38, 1185-1205, 2004.
- 410 Dominguez-Rodriguez, A., Rodriguez, S., Abreu-Gonzalez, P., Avanzas, P., and Juarez-Prera, R. A.: Black carbon exposure, oxidative stress markers and major adverse cardiovascular events in patients with acute coronary syndromes, *Int J Cardiol*, 188, 47-49, 10.1016/j.ijcard.2015.04.023, 2015.  
Edenhofer, O., and Seyboth, K.: Intergovernmental Panel on Climate Change (IPCC), *Encyclopedia of Energy Natural Resource & Environmental Economics*, 26, 48-56, 2013.
- 415 Flanner, M. G., Zender, C. S., Randerson, J. T., and Rasch, P. J.: Present-day climate forcing and response from black carbon in snow, *J. Geophys. Res.-Atmos.*, 112, 2007.  
Gao, R. S., Schwarz, J. P., Kelly, K. K., Fahey, D. W., Watts, L. A., Thompson, T. L., Spackman, J. R., Slowik, J. G., Cross, E. S., Han, J. H., Davidovits, P., Onasch, T. B., and Worsnop, D. R.: A novel method for estimating light-scattering properties of soot aerosols using a modified single-particle soot photometer, *Aerosol Science and Technology*, 41, 125-135,  
420 10.1080/02786820601118398, 2007.  
Hallquist, M., Wenger, J. C., Baltensperger, U., Rudich, Y., Simpson, D., Claeys, M., Dommen, J., Donahue, N. M., George, C., Goldstein, A. H., Hamilton, J. F., Herrmann, H., Hoffmann, T., Iinuma, Y., Jang, M., Jenkin, M. E., Jimenez, J. L., Kiendler-Scharr, A., Maenhaut, W., McFiggans, G., Mentel, T. F., Monod, A., Prevot, A. S. H., Seinfeld, J. H., Surratt, J. D., Szmigielski, R., and Wildt, J.: The formation, properties and impact of secondary organic aerosol: current and emerging issues, *Atmospheric Chemistry and Physics*, 9, 5155-5236, DOI 10.5194/acp-9-5155-2009, 2009.
- 425 Han, C., Li, S. M., Liu, P., and Lee, P.: Size Dependence of the Physical Characteristics of Particles Containing Refractory Black Carbon in Diesel Vehicle Exhaust, *Environ Sci Technol*, 53, 137-145, 10.1021/acs.est.8b04603, 2019.  
Laborde, M., Crippa, M., Tritscher, T., Juranyi, Z., Decarlo, P. F., Temime-Roussel, B., Marchand, N., Eckhardt, S., Stohl, A., Baltensperger, U., Prevot, A. S. H., Weingartner, E., and Gysel, M.: Black carbon physical properties and mixing state in the

- 430 European megacity Paris, *Atmospheric Chemistry and Physics*, 13, 5831-5856, 10.5194/acp-13-5831-2013, 2013.  
 Lack, D. A., Langridge, J. M., Bahreini, R., Cappa, C. D., Middlebrook, A. M., and Schwarz, J. P.: Brown carbon and internal mixing in biomass burning particles, *P Natl Acad Sci USA*, 109, 14802-14807, 2012.
- Lan, Z. J., Huang, X. F., Yu, K. Y., Sun, T. L., Zeng, L. W., and Hu, M.: Light absorption of black carbon aerosol and its enhancement by mixing state in an urban atmosphere in South China, *Atmos Environ*, 69, 118-123,  
 435 10.1016/j.atmosenv.2012.12.009, 2013.
- Lelieveld, J., Evans, J. S., Fnais, M., Giannadaki, D., and Pozzer, A.: The contribution of outdoor air pollution sources to premature mortality on a global scale, *Nature*, 525, 367-+, 10.1038/nature15371, 2015.
- Liu, D., Allan, J., Whitehead, J., Young, D., Flynn, M., Coe, H., McFiggans, G., Fleming, Z. L., and Bandy, B.: Ambient black carbon particle hygroscopic properties controlled by mixing state and composition, *Atmospheric Chemistry and Physics*, 13,  
 440 2015-2029, 10.5194/acp-13-2015-2013, 2013.
- Liu, D., Allan, J. D., Young, D. E., Coe, H., Beddows, D., Fleming, Z. L., Flynn, M. J., Gallagher, M. W., Harrison, R. M., Lee, J., Prevot, A. S. H., Taylor, J. W., Yin, J., Williams, P. I., and Zotter, P.: Size distribution, mixing state and source apportionment of black carbon aerosol in London during wintertime, *Atmospheric Chemistry and Physics*, 14, 10061-10084, 10.5194/acp-14-10061-2014, 2014.
- 445 Liu, D. T., Whitehead, J., Alfarra, M. R., Reyes-Villegas, E., Spracklen, D. V., Reddington, C. L., Kong, S. F., Williams, P. I., Ting, Y. C., Haslett, S., Taylor, J. W., Flynn, M. J., Morgan, W. T., McFiggans, G., Coe, H., and Allan, J. D.: Black-carbon absorption enhancement in the atmosphere determined by particle mixing state, *Nat Geosci*, 10, 184-U132, 10.1038/Ngeo2901, 2017.
- Liu, Z. R., Hu, B., Ji, D. S., Wang, Y. H., Wang, M. X., and Wang, Y. S.: Diurnal and seasonal variation of the PM<sub>2.5</sub> apparent particle density in Beijing, China, *Atmos Environ*, 120, 328-338, 10.1016/j.atmosenv.2015.09.005, 2015.
- 450 Londahl, J., Pagels, J., Boman, C., Swietlicki, E., Massling, A., Rissler, J., Blomberg, A., Bohgard, M., and Sandstrom, T.: Deposition of biomass combustion aerosol particles in the human respiratory tract, *Inhal Toxicol*, 20, 923-933, 10.1080/08958370802087124, 2008.
- Malloy, Q. G. J., Nakao, S., Qi, L., Austin, R., Stothers, C., Hagino, H., and Cocker, D. R.: Real-Time Aerosol Density Determination Utilizing a Modified Scanning Mobility Particle Sizer Aerosol Particle Mass Analyzer System, *Aerosol Science and Technology*, 43, 673-678, Pii 910340704  
 455 10.1080/02786820902832960, 2009.
- Momenimovahed, A., and Olfert, J. S.: Effective Density and Volatility of Particles Emitted from Gasoline Direct Injection Vehicles and Implications for Particle Mass Measurement, *Aerosol Science and Technology*, 49, 1051-1062,  
 460 10.1080/02786826.2015.1094181, 2015.
- Moteki, N., and Kondo, Y.: Effects of mixing state on black carbon measurements by laser-induced incandescence, *Aerosol Science and Technology*, 41, 398-417, 10.1080/02786820701199728, 2007.
- Moteki, N., Kondo, Y., Oshima, N., Takegawa, N., Koike, M., Kita, K., Matsui, H., and Kajino, M.: Size dependence of wet removal of black carbon aerosols during transport from the boundary layer to the free troposphere, *Geophysical Research Letters*, 39, Artn L13802  
 465 10.1029/2012gl052034, 2012.
- Nakayama, T., Matsumi, Y., Sato, K., Imamura, T., Yamazaki, A., and Uchiyama, A.: Laboratory studies on optical properties of secondary organic aerosols generated during the photooxidation of toluene and the ozonolysis of alpha-pinene, *J. Geophys. Res.-Atmos.*, 115, Artn D24204  
 470 10.1029/2010jd014387, 2010.
- Olfert, J. S., and Collings, N.: New method for particle mass classification - the Couette centrifugal particle mass analyzer, *J Aerosol Sci*, 36, 1338-1352, 10.1016/j.jaerosci.2005.03.006, 2005.
- Pagels, J., Khalizov, A. F., McMurry, P. H., and Zhang, R. Y.: Processing of Soot by Controlled Sulphuric Acid and Water Condensation Mass and Mobility Relationship, *Aerosol Science and Technology*, 43, 629-640, Pii 910341827  
 475 10.1080/02786820902810685, 2009.
- Pan, X. L., Kanaya, Y., Taketani, F., Miyakawa, T., Inomata, S., Komazaki, Y., Tanimoto, H., Wang, Z., Uno, I., and Wang, Z. F.: Emission characteristics of refractory black carbon aerosols from fresh biomass burning: a perspective from laboratory experiments, *Atmospheric Chemistry and Physics*, 17, 13001-13016, 10.5194/acp-17-13001-2017, 2017.
- Pan, X. L., Ge, B. Z., Wang, Z., Tian, Y., Liu, H., Wei, L. F., Yue, S. Y., Uno, I., Kobayashi, H., Nishizawa, T., Shimizu, A., Fu,

- 480 P. Q., and Wang, Z. F.: Synergistic effect of water-soluble species and relative humidity on morphological changes in aerosol particles in the Beijing megacity during severe pollution episodes, *Atmospheric Chemistry and Physics*, 19, 219-232, 10.5194/acp-19-219-2019, 2019.
- Peng, J. F., Hu, M., Guo, S., Du, Z. F., Zheng, J., Shang, D. J., Zamora, M., Zeng, L. M., Shao, M., Wu, Y. S., Zheng, J., Wang, Y., Glen, C., Collins, D., Molina, M., and Zhang, R. Y.: Markedly enhanced absorption and direct radiative forcing of black carbon under polluted urban environments, *Abstr Pap Am Chem S*, 252, 2016.
- 485 Qiao, K., Wu, Z. J., Pei, X. Y., Liu, Q. Y., Shang, D. J., Zheng, J., Du, Z. F., Zhu, W. F., Wu, Y. S., Lou, S. R., Guo, S., Chan, C. K., Pathak, R. K., Hallquist, M., and Hu, M.: Size-resolved effective density of submicron particles during summertime in the rural atmosphere of Beijing, China, *J Environ Sci-China*, 73, 69-77, 10.1016/j.jes.2018.01.012, 2018.
- Qiu, C., Khalizov, A. F., Hogan, B., Petersen, E. L., and Zhang, R. Y.: High Sensitivity of Diesel Soot Morphological and Optical Properties to Combustion Temperature in a Shock Tube, *Environ Sci Technol*, 48, 6444-6452, 10.1021/es405589d, 2014.
- 490 Raaschou-Nielsen, O., Andersen, Z. J., Beelen, R., Samoli, E., Stafoggia, M., Weinmayr, G., Hoffmann, B., Fischer, P., Nieuwenhuijsen, M. J., Brunekreef, B., Xun, W. W., Katsouyanni, K., Dimakopoulou, K., Sommar, J., Forsberg, B., Modig, L., Oudin, A., Oftedal, B., Schwarze, P. E., Nafstad, P., De Faire, U., Pedersen, N. L., Ostenson, C. G., Fratiglioni, L., Penell, J., Korek, M., Pershagen, G., Eriksen, K. T., Sorensen, M., Tjonneland, A., Ellermann, T., Eeftens, M., Peeters, P. H., Meliefste, K., Wang, M., Bueno-de-Mesquita, B., Key, T. J., de Hoogh, K., Concin, H., Nagel, G., Vilier, A., Grioni, S., Krogh, V., Tsai, M. Y., Ricceri, F., Sacerdote, C., Galassi, C., Migliore, E., Ranzi, A., Cesaroni, G., Badaloni, C., Forastiere, F., Tamayo, I., Amiano, P., Dorronsoro, M., Trichopoulou, A., Bamia, C., Vineis, P., and Hoek, G.: Air pollution and lung cancer incidence in 17 European cohorts: prospective analyses from the European Study of Cohorts for Air Pollution Effects (ESCAPE), *Lancet Oncol*, 14, 813-822, 10.1016/s1470-2045(13)70279-1, 2013.
- 500 Ramanathan, V., and Carmichael, G.: Global and regional climate changes due to black carbon, *Nat Geosci*, 36, págs. 335-358, 2008.
- Rissler, J., Nordin, E. Z., Eriksson, A. C., Nilsson, P. T., Frosch, M., Sporre, M. K., Wierzbicka, A., Svenningsson, B., Londahl, J., Messing, M. E., Sjogren, S., Hemmingsen, J. G., Loft, S., Pagels, J. H., and Swietlicki, E.: Effective Density and Mixing State of Aerosol Particles in a Near-Traffic Urban Environment, *Environ Sci Technol*, 48, 6300-6308, 10.1021/es5000353, 2014.
- 505 Schnaiter, M., Horvath, H., Mohler, O., Naumann, K. H., Saathoff, H., and Schock, O. W.: UV-VIS-NIR spectral optical properties of soot and soot-containing aerosols, *J Aerosol Sci*, 34, 1421-1444, 10.1016/S0021-8502(03)00361-6, 2003.
- Shiraiwa, M., Kondo, Y., Moteki, N., Takegawa, N., Sahu, L., Takami, A., Hatakeyama, S., Yonemura, S., and Blake, D.: Radiative impact of mixing state of black carbon aerosol in Asian outflow, *Journal of Geophysical Research: Atmospheres*, 113, 2008.
- 510 Shiraiwa, M., Kondo, Y., Iwamoto, T., and Kita, K.: Amplification of Light Absorption of Black Carbon by Organic Coating, *Aerosol Science and Technology*, 44, 46-54, 2010.
- Sun, Y. L., Wang, Z. F., Wild, O., Xu, W. Q., Chen, C., Fu, P. Q., Du, W., Zhou, L. B., Zhang, Q., Han, T. T., Wang, Q. Q., Pan, X. L., Zheng, H. T., Li, J., Guo, X. F., Liu, J. G., and Worsnop, D. R.: "APEC Blue": Secondary Aerosol Reductions from Emission Controls in Beijing, *Sci Rep-Uk*, 6, ARTN 20668, 10.1038/srep20668, 2016.
- 515 Tavakoli, F., and Olfert, J. S.: Determination of particle mass, effective density, mass-mobility exponent, and dynamic shape factor using an aerodynamic aerosol classifier and a differential mobility analyzer in tandem, *J Aerosol Sci*, 75, 35-42, 10.1016/j.jaerosci.2014.04.010, 2014.
- Taylor, J. W., Allan, J. D., Liu, D., Flynn, M., Weber, R., Zhang, X., Lefer, B. L., Grossberg, N., Flynn, J., and Coe, H.: Assessment of the sensitivity of core/shell parameters derived using the single-particle soot photometer to density and refractive index, *Atmos Meas Tech*, 8, 1701-1718, 10.5194/amt-8-1701-2015, 2015.
- 520 Toon, O. B., Pollack, J. B., and Khare, B. N.: Optical-Constants of Several Atmospheric Aerosol Species - Ammonium-Sulfate, Aluminum-Oxide, and Sodium-Chloride, *J Geophys Res-Oc Atm*, 81, 5733-5748, DOI 10.1029/JC081i033p05733, 1976.
- Turpin, B. J., and Lim, H. J.: Species contributions to PM<sub>2.5</sub> mass concentrations: Revisiting common assumptions for estimating organic mass, *Aerosol Science and Technology*, 35, 602-610, Doi 10.1080/02786820119445, 2001.
- 525 Wang, Q. Y., Huang, R. J., Cao, J. J., Han, Y. M., Wang, G. H., Li, G. H., Wang, Y. C., Dai, W. T., Zhang, R. J., and Zhou, Y. Q.: Mixing State of Black Carbon Aerosol in a Heavily Polluted Urban Area of China: Implications for Light Absorption

- 530 Enhancement, *Aerosol Science and Technology*, 48, 689-697, 10.1080/02786826.2014.917758, 2014.  
Wang, Q. Y., Huang, R. J., Zhao, Z. Z., Cao, J. J., Ni, H. Y., Tie, X. X., Zhao, S. Y., Su, X. L., Han, Y. M., Shen, Z. X., Wang, Y. C., Zhang, N. N., Zhou, Y. Q., and Corbin, J. C.: Physicochemical characteristics of black carbon aerosol and its radiative impact in a polluted urban area of China, *J. Geophys. Res.-Atmos.*, 121, 12505-12519, 10.1002/2016jd024748, 2016.  
Wang, Y. Y., Liu, F. S., He, C. L., Bi, L., Cheng, T. H., Wang, Z. L., Zhang, H., Zhang, X. Y., Shi, Z. B., and Li, W. J.: Fractal Dimensions and Mixing Structures of Soot Particles during Atmospheric Processing, *Environ Sci Tech Let*, 4, 487-493, 10.1021/acs.estlett.7b00418, 2017.
- 535 Wu, Y., Cheng, T. H., Liu, D. T., Allan, J. D., Zheng, L. J., and Chen, H.: Light Absorption Enhancement of Black Carbon Aerosol Constrained by Particle Morphology, *Environ Sci Technol*, 52, 6912-6919, 10.1021/acs.est.8b00636, 2018.  
Wu, Y. F., Zhang, R. J., Tian, P., Tao, J., Hsu, S. C., Yan, P., Wang, Q. Y., Cao, J. J., Zhang, X. L., and Xia, X. G.: Effect of ambient humidity on the light absorption amplification of black carbon in Beijing during January 2013, *Atmos Environ*, 124, 217-223, 10.1016/j.atmosenv.2015.04.041, 2016.
- 540 Wu, Y. F., Wang, X. J., Tao, J., Huang, R. J., Tian, P., Cao, J. J., Zhang, L. M., Ho, K. F., Han, Z. W., and Zhang, R. J.: Size distribution and source of black carbon aerosol in urban Beijing during winter haze episodes, *Atmospheric Chemistry and Physics*, 17, 7965-7975, 10.5194/acp-17-7965-2017, 2017.
- 545 Xue, H. X., Khalizov, A. F., Wang, L., Zheng, J., and Zhang, R. Y.: Effects of Coating of Dicarboxylic Acids on the Mass-Mobility Relationship of Soot Particles, *Environ Sci Technol*, 43, 2787-2792, 10.1021/es803287v, 2009.  
Zhang, R. Y., Khalizov, A. F., Pagels, J., Zhang, D., Xue, H. X., and McMurry, P. H.: Variability in morphology, hygroscopicity, and optical properties of soot aerosols during atmospheric processing, *P Natl Acad Sci USA*, 105, 10291-10296, 10.1073/pnas.0804860105, 2008.
- 550 Zhang, Y. X., Zhang, Q., Cheng, Y. F., Su, H., Kecorius, S., Wang, Z. B., Wu, Z. J., Hu, M., Zhu, T., Wiedensohler, A., and He, K. B.: Measuring the morphology and density of internally mixed black carbon with SP2 and VTDMA: new insight into the absorption enhancement of black carbon in the atmosphere, *Atmos Meas Tech*, 9, 1833-1843, 10.5194/amt-9-1833-2016, 2016.  
Zhang, Y. X., Su, H., Ma, N., Li, G., Kecorius, S., Wang, Z. B., Hu, M., Zhu, T., He, K. B., Wiedensohler, A., Zhang, Q., and Cheng, Y. F.: Sizing of Ambient Particles From a Single-Particle Soot Photometer Measurement to Retrieve Mixing State of  
555 Black Carbon at a Regional Site of the North China Plain, *J. Geophys. Res.-Atmos.*, 123, 12778-12795, 10.1029/2018jd028810, 2018.

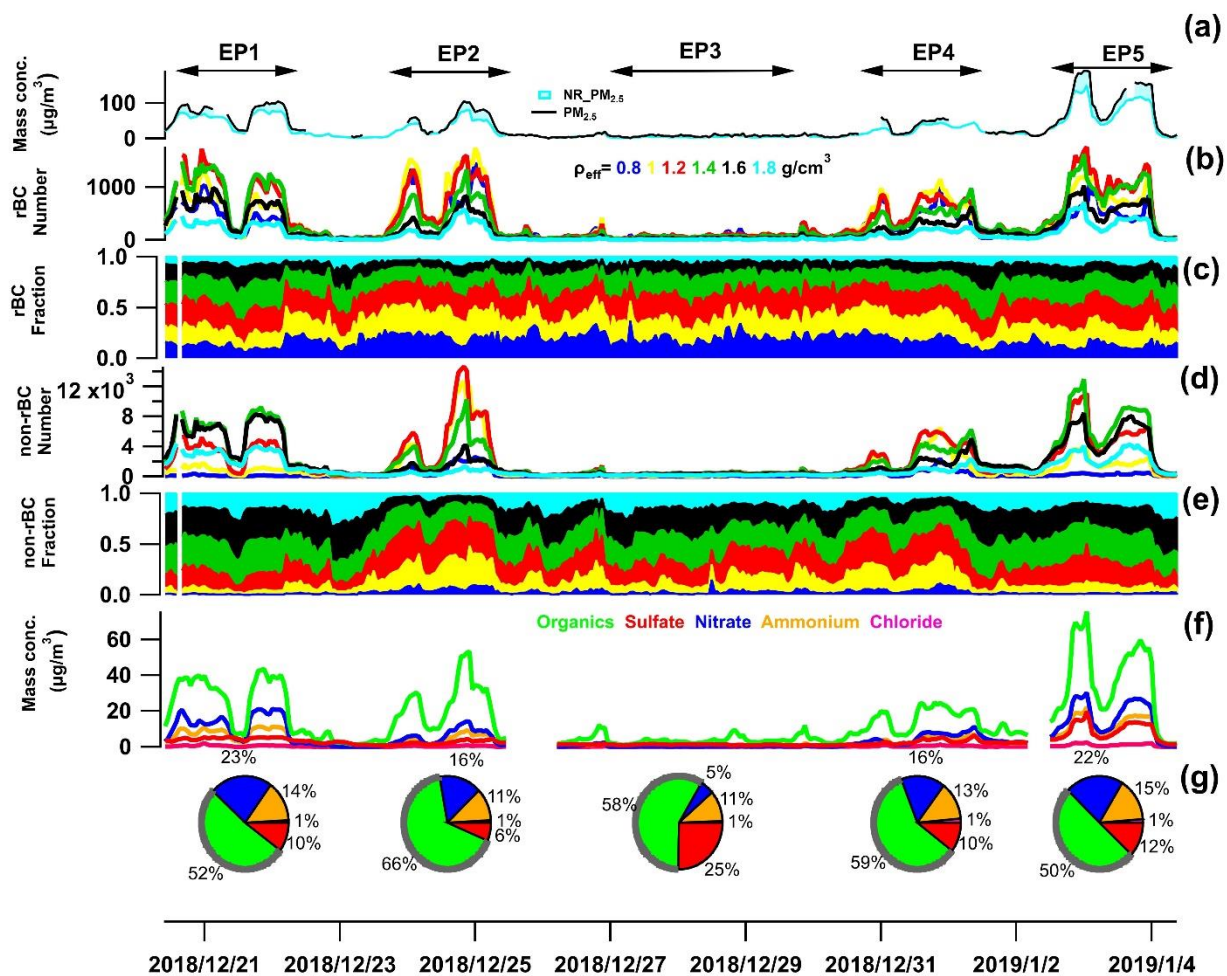
**Table 1. Abbreviations and symbols used in this paper**

Abbreviation/symbols	Full name/explanation
$\rho_{\text{non-rBC}}$ & $\rho_{\text{non-rBC}}$	Effective density of non-rBC particles (rBC-containing particles)
$\rho_{\text{non-rBC,bulk}}$ & $\rho_{\text{rBC,bulk}}$	Effective density of bulk non-rBC particles (rBC-containing particles) using the weighted average method. $\rho_{\text{non-rBC,bulk}}$ is different from $\rho_{\text{non-rBC}}$ , since the number distribution of non-rBC particles with different $\rho_{\text{non-rBC}}$ values is considered to reflect the effective density of bulk non-rBC.
SP2	Single particle soot photometer (DMT Technologies)
DMA	Differential mobility analyzer (TSI Inc.)
CPMA	Couette centrifugal particle mass analyzer (Cambustion, Ltd.)
CPC	Condensation particle counter (TSI Inc.)
rBC	Refractory black carbon determined by the SP2 through the laser-induced incandescence method
$D_{\text{mob}}$	Mobility diameter selected by the DMA
$D_{\text{opt}}$	Optical diameter derived from the SP2 scattering signal
$\chi$	Dynamic shape factor of particles representing the particle regularity
$R_{\text{void}}$	Void volume ratio in a particle representing the particle compactness
$M_{\text{R}}$	The mass ratio of coatings to the rBC core representing the coating thickness
S/C ratio	The ratio of the diameter of rBC-containing particles to the diameter of the rBC core representing the coating thickness
$\sigma_{\text{SC}}$	Scattering cross-section of rBC-containing particles
MAC	Mass absorption cross-section of rBC-containing particles

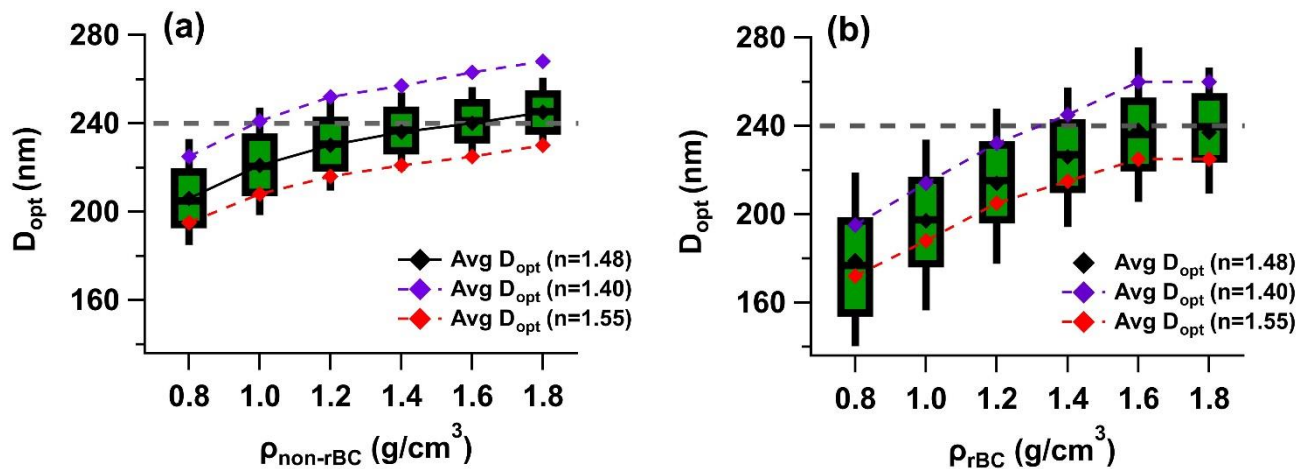
**Table 2. Brief summary of the effective density and dynamic shape factor of rBC-containing particles**

Particle type	Shape factor*	Effective density* (g/cm <sup>3</sup> )	Description	Reference
ambient	-	1.42 (0.39)	The $\rho_{\text{eff}}$ distribution exhibits a bimodal pattern. The left peak is contributed by fresh soot with a $\rho_{\text{eff}}$ of 0.39 g/cm <sup>3</sup> .	(Rissler et al., 2014)
ambient	-	1.50 (0.8)	Similar bimodal $\rho_{\text{eff}}$ distribution.	(Qiao et al., 2018)
non-rBC (dioctyl sebacate)	1.03	0.931	The shape factor is nearly 1 for non-rBC particles.	(Tavakoli and Olfert, 2014)
rBC-containing particles	2.10	1.00	rBC-containing particles from a diesel truck.	(Han et al., 2019)
	4	0.18	rBC-containing particles generated from a propane flame.	(Xue et al., 2009)
	1.80	0.70	Propane flame rBC-containing particles coated with glutaric acid.	
	1.87	0.50	rBC-containing particles generated from a methane flame.	(Tavakoli and Olfert, 2014)
	1.03 - 2.79	1.36 - 0.25	Diesel exhaust rBC-containing particles with different combustion temperatures; the rBC-containing particles were more compact from the lower temperature combustion condition.	(Qiu et al., 2014)
1 - 2.8	1.4 - 0.25	Laboratory-generated rBC-containing particles with different aging times; the rBC-containing particles were more compact when undergoing a long aging process.	(Peng et al., 2016)	

\*The effective density and shape factor counted in this table is for rBC-containing particles with a  $D_{\text{mob}}=240\pm 20$  nm.



570 **Figure 1.** Time series of (a) the PM<sub>2.5</sub> mass concentration, (b) number counts of rBC-containing particles with different effective densities, (c) number fractions of rBC-containing particles with different effective densities, (d) number counts of non-rBC particles with different effective densities, (e) number fractions of non-rBC particles with different effective densities, (f) mass concentrations of aerosol species, including organics, sulfate, nitrate, ammonium, and chloride, in NR-PM<sub>2.5</sub> and (g) mass fractions of aerosol species in NR-PM<sub>2.5</sub> during the five episodes denoted at the top of the graph.



575 Figure 2. The optical diameters of particles with different effective densities. (a) Non-rBC particles and (b) BC-containing particles. (The black lines in the middle signify the medians; the black markers in the middle denote the means; the upper and lower bounds of the box denote the 75th and 25th percentiles, respectively; and the upper and lower whiskers denote the 90th and 10th percentiles, respectively.) The blue and red dashed lines denote the average optical diameters from different assumptions of the refractive index. The grey dashed line denotes the mobility diameter ( $D_{mob} = 240$  nm) selected by DMA.

580

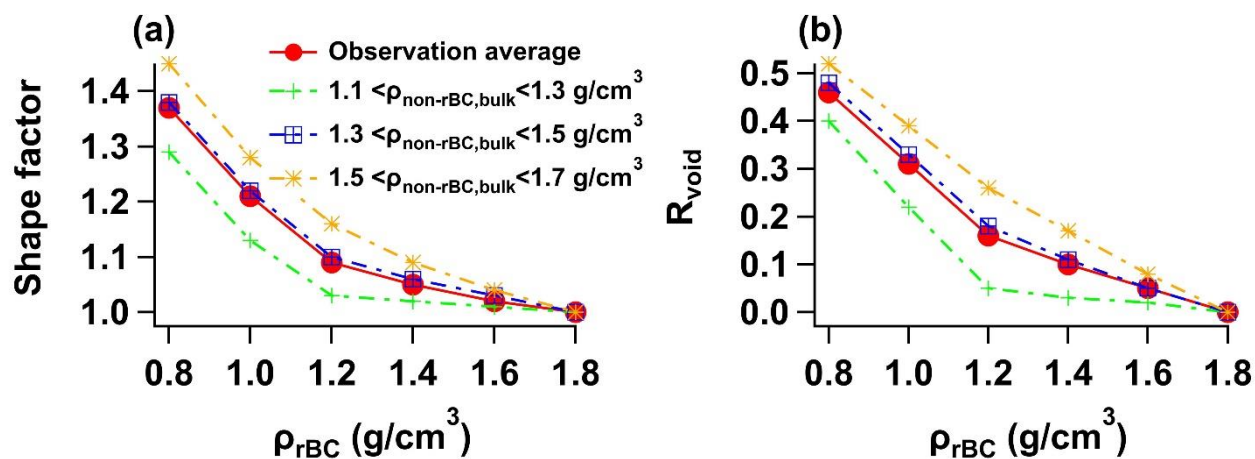
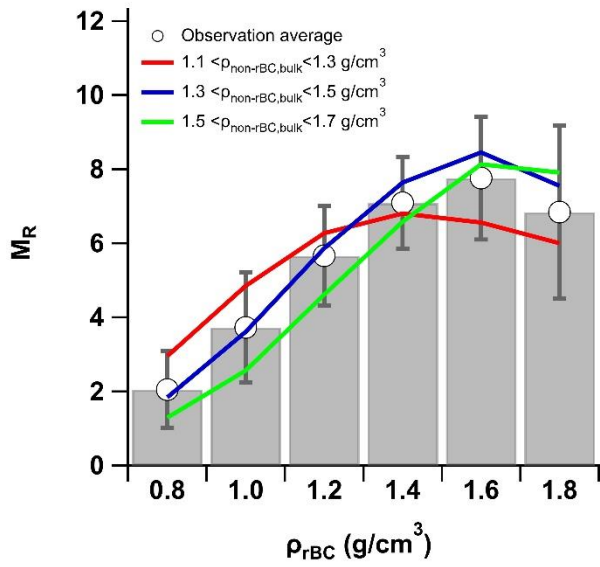
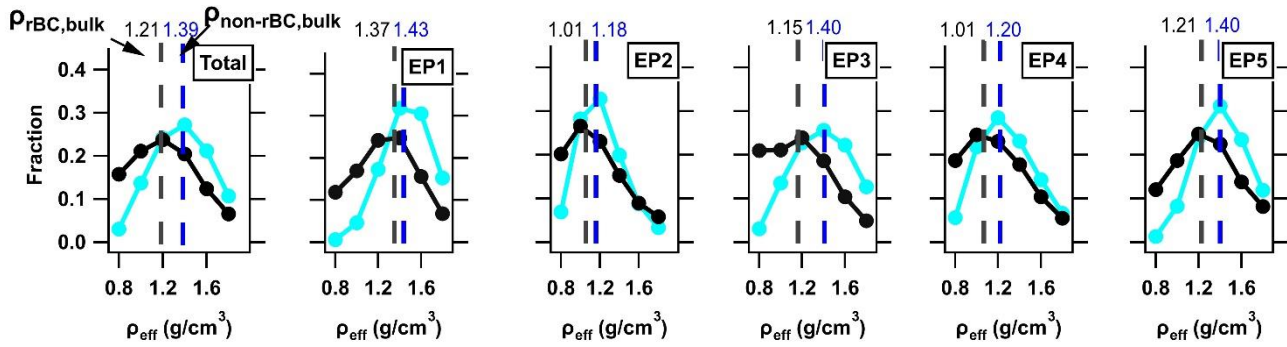


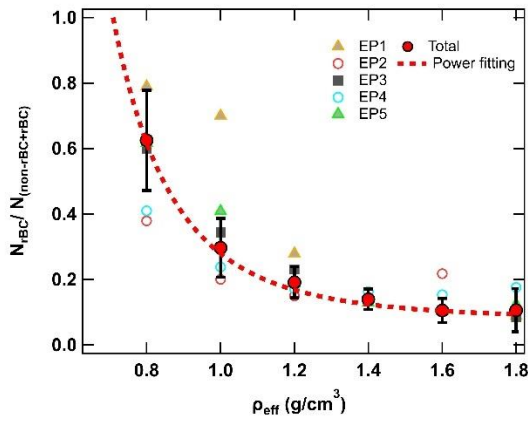
Figure 3. The shape factor and void fraction of BC-containing particles under different effective densities.



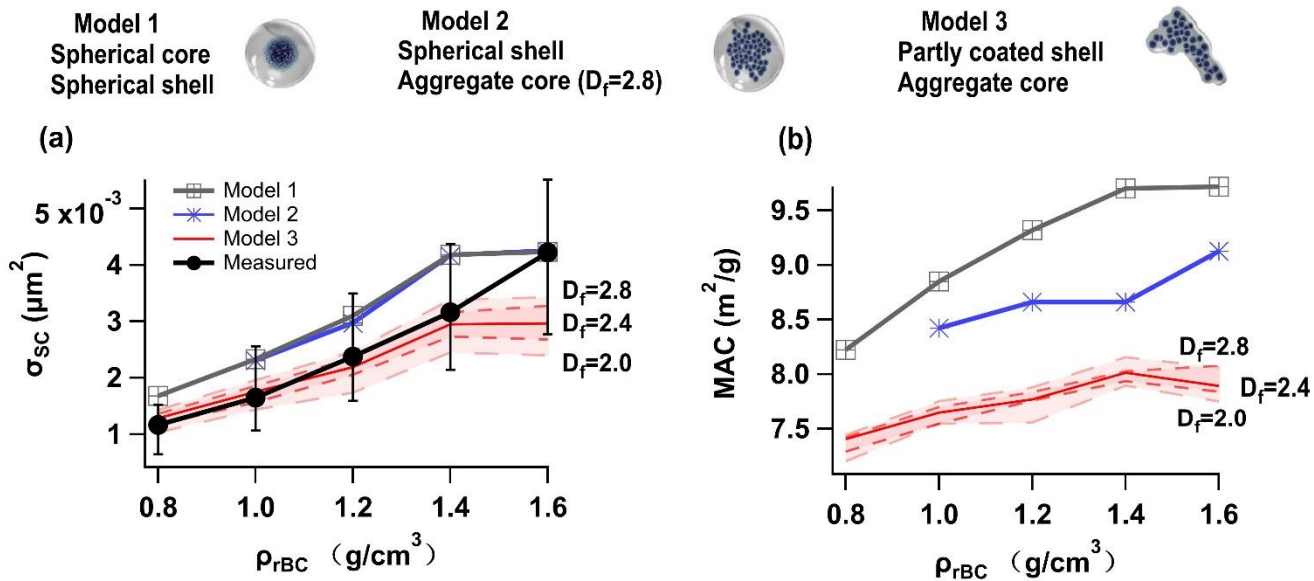
585 Figure 4. Variation of mass ratio ( $M_R$ ) of coatings to rBC as a function of  $\rho_{rBC}$ .



590 Figure 5. Number distributions of rBC-containing particles (black lines) and non-rBC particles (blue lines) with different effective densities during different episodes. The black dashed line denotes the effective density of bulk rBC-containing particles, and the blue dashed line denotes the effective density of bulk non-rBC particles.



595 Figure 6. Number fractions of rBC-containing particles in the total particles (rBC-containing and non-rBC particles) under different effective densities.



600 Figure 7. (a) The scattering cross-section of BC-containing particles at the 1064 nm wavelength predicted by different models and measured by the SP2 under different effective densities. (b) The mass absorption cross-section at the 532 nm wavelength predicted by different models under different effective densities. Model 3 was used with various assumptions of the core fractal dimension ( $D_f=2.0, 2.2, 2.4, 2.6, \text{ and } 2.8$ ) as denoted in the graph.

# Supplementary

605 Table. S1 Optical characteristics from the different models

MODEL	DF	DC	DP	CEXT	CABS	CSCA	MEC1064	MAC1064	MSC1064	MAC532	S/C RATIO
C	2	127	194	0.008249	0.007222	0.001028	4.273068	3.740848	0.53225	7.200429	1.527559
C	2.2	127	194	0.008481	0.00731	0.001171	4.392802	3.786476	0.606372	7.288254	1.527559
C	2.4	127	194	0.008713	0.007426	0.001287	4.512995	3.846496	0.666484	7.403781	1.527559
C	2.6	127	194	0.008807	0.007442	0.001365	4.562144	3.85507	0.706998	7.420285	1.527559
C	2.8	127	194	0.008894	0.007465	0.001429	4.607159	3.867013	0.740192	7.443273	1.527559
B	2.6	118	211	0.009052	0.006749	0.002303	5.845469	4.358303	1.487188	8.388915	1.788136
B	2.8	118	211	0.009081	0.006776	0.002306	5.864437	4.37569	1.488904	8.422382	1.788136
C	2	118	211	0.007509	0.00607	0.001438	4.848982	3.920012	0.928948	7.545286	1.788136
C	2.2	118	211	0.007634	0.00607	0.001565	4.930047	3.919786	1.010442	7.544851	1.788136
C	2.4	118	211	0.007902	0.006153	0.00175	5.103241	3.973302	1.129984	7.64786	1.788136
C	2.6	118	211	0.00805	0.006192	0.001859	5.198757	3.998593	1.200255	7.696539	1.788136
C	2.8	118	211	0.008196	0.006236	0.00196	5.292919	4.02727	1.265694	7.751738	1.788136
B	2.4	111	225	0.008644	0.00569	0.002954	6.706476	4.414534	2.292127	8.497148	2.027027
B	2.6	111	225	0.008784	0.005813	0.002971	6.814749	4.509543	2.305237	8.680022	2.027027
B	2.8	111	225	0.008772	0.005799	0.002973	6.805804	4.499055	2.306625	8.659835	2.027027
C	2	111	225	0.006794	0.005059	0.001735	5.270542	3.92499	1.345706	7.554867	2.027027
C	2.2	111	225	0.007256	0.005202	0.002054	5.629294	4.036039	1.593255	7.768617	2.027027
C	2.4	111	225	0.007386	0.005195	0.002191	5.729856	4.030178	1.699492	7.757336	2.027027
C	2.6	111	225	0.007596	0.005246	0.002349	5.892728	4.07028	1.822603	7.834523	2.027027
C	2.8	111	225	0.007747	0.005275	0.002472	6.010565	4.092798	1.917643	7.877867	2.027027
B	2.2	110	238	0.010017	0.005874	0.004144	7.985556	4.682386	3.303418	9.012713	2.163636
B	2.4	110	238	0.010097	0.005946	0.004151	8.049037	4.740193	3.309057	9.123981	2.163636
B	2.6	110	238	0.010119	0.005962	0.004156	8.066415	4.752961	3.313348	9.148556	2.163636
B	2.8	110	238	0.010234	0.006061	0.004174	8.158623	4.831337	3.327179	9.299416	2.163636
C	2	110	238	0.007595	0.005145	0.00245	6.054156	4.101122	1.952927	7.893889	2.163636
C	2.2	110	238	0.007898	0.005171	0.002727	6.296024	4.122401	2.173517	7.934847	2.163636
C	2.4	110	238	0.008168	0.005221	0.002946	6.510939	4.162121	2.348676	8.011301	2.163636
C	2.6	110	238	0.008391	0.00523	0.003161	6.689326	4.169569	2.519899	8.025636	2.163636
C	2.8	110	238	0.0087	0.005315	0.003385	6.93545	4.236597	2.698676	8.154652	2.163636
B	2.2	112	239	0.010308	0.006093	0.004215	7.784914	4.601424	3.183592	8.856876	2.133929
B	2.4	112	239	0.010509	0.006264	0.004245	7.936702	4.730851	3.205648	9.105998	2.133929
B	2.6	112	239	0.010464	0.006224	0.00424	7.902482	4.700357	3.202294	9.047304	2.133929
B	2.8	112	239	0.010527	0.006277	0.00425	7.950255	4.740337	3.210019	9.124258	2.133929
C	2	112	239	0.007729	0.005331	0.002398	5.837076	4.026119	1.811025	7.749522	2.133929
C	2.2	112	239	0.008068	0.005392	0.002676	6.093219	4.072197	2.021225	7.838215	2.133929
C	2.4	112	239	0.008395	0.005429	0.002966	6.340214	4.100319	2.239726	7.892343	2.133929
C	2.6	112	239	0.008832	0.005556	0.003276	6.670218	4.196203	2.47415	8.076902	2.133929
C	2.8	112	239	0.008973	0.005545	0.003428	6.776944	4.187733	2.589144	8.060598	2.133929



Cases 1-5, Models A/B/C from left to right

The fractal prefactor ( $k_0$ ) is assumed to be 1.2. The monomer size ( $a$ ) is assumed to be  $0.02 \mu\text{m}$ . The monomer number ( $N_s$ ) is calculated as the volume-equivalent radii of BC. The wavelength is  $1.064 \mu\text{m}$ .

610

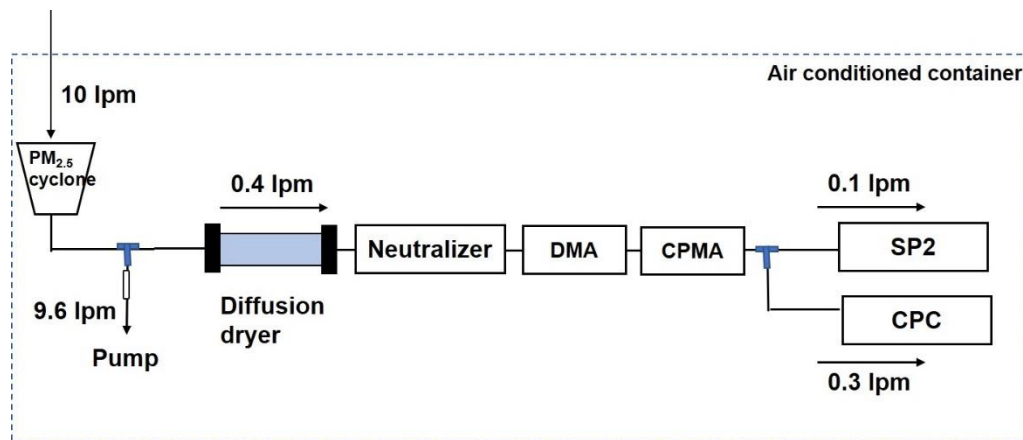
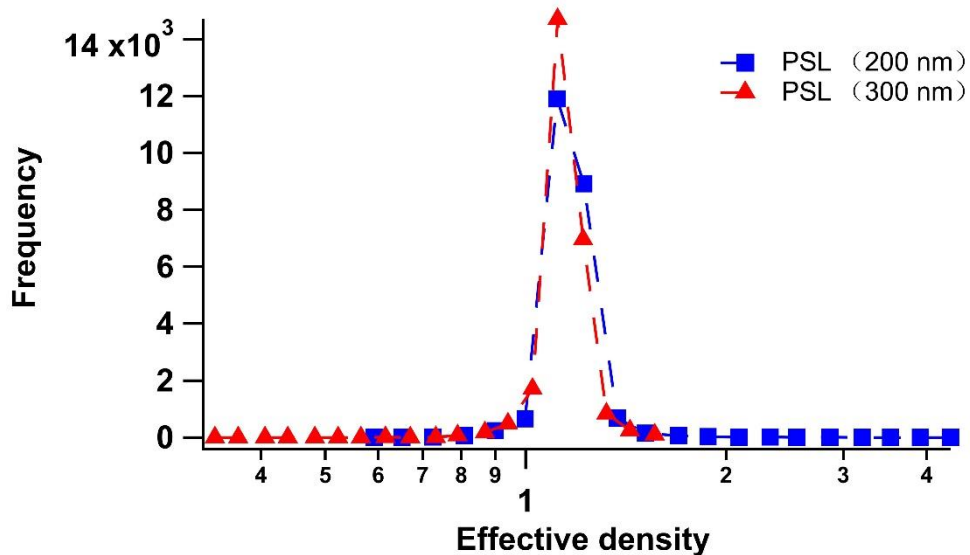


Figure. S1 Schematic diagram of the measurement system.



615 Figure. S2 The effective density distribution of PSL determined by the DMA+CPMA tandem system.

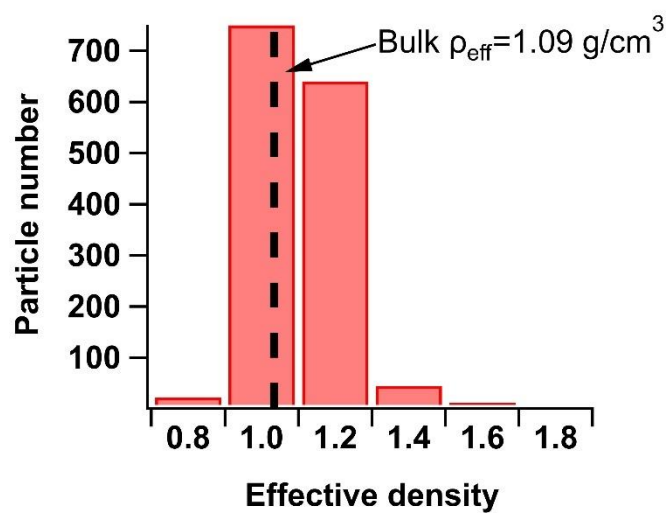


Figure. S3 The weighted average method used to determine the bulk aerosol density of PSL.

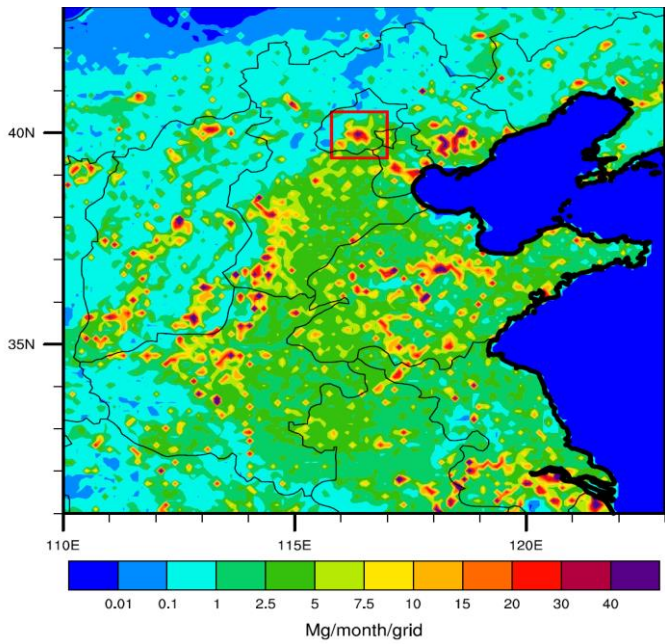


Figure. S4 The emission of rBC in in eastern-central China. The red box denotes the geographical location of the observation site.

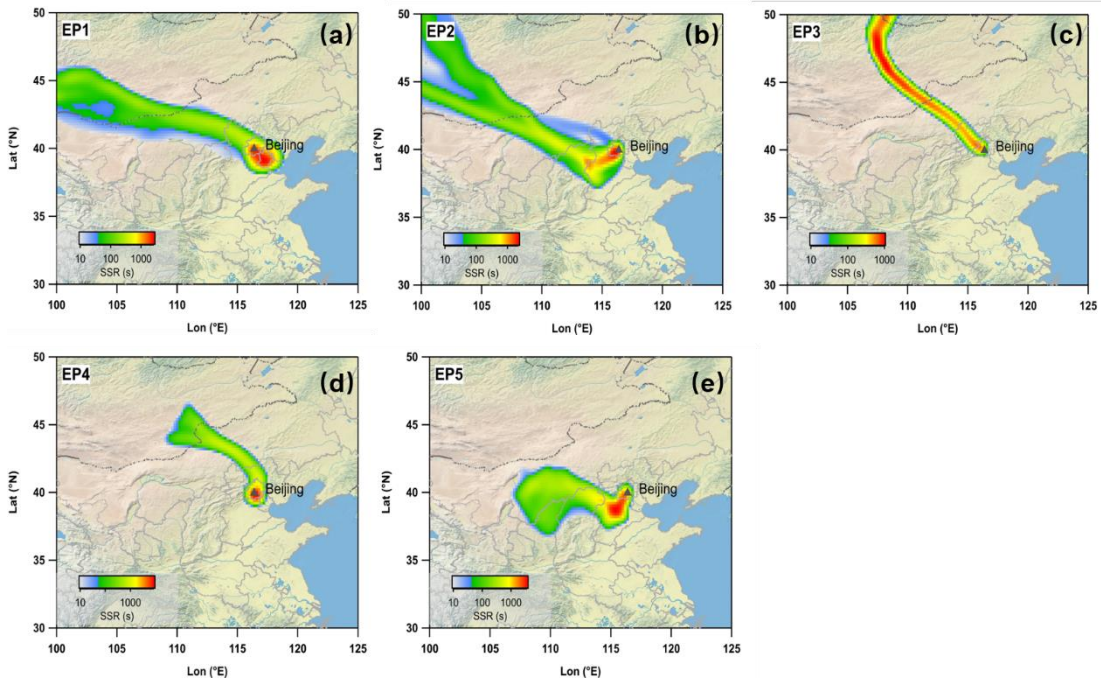
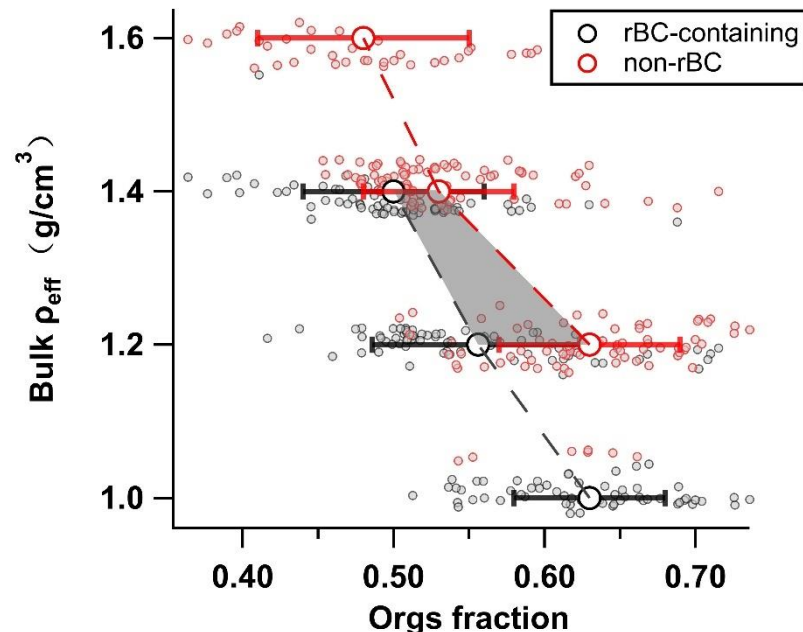


Figure. S5 The 24 h backward trajectories during the five episodes. SSR is the residence time of particles in each cell. The FLEXPART (FLEXible PARTicle) dispersion model (<https://www.flexpart.eu>, last access: 15 June 2018) developed by the Norwegian Institute for Air Research was used to predicted the backward trajectory. Global Data Assimilation System (GDAS) with

1°×1° resolution was used as the meteorology input for FLEXPART. Air samples were released at 50m above ground level and the simulation time of backward trajectory is 1 day.



630 Figure. S6 The relationship between the bulk effective density and the organic mass fraction in the NR-PM<sub>2.5</sub>.

#### Uncertainty analyze:

The physical parameters directly measured by the tandem system is the mass of rBC-containing particle ( $M_p$ ), the mass of rBC core ( $M_{rBC}$ ) and the mobility diameter of rBC-containing particle ( $D_{mob}$ ).

$M_p$  is selected by CPMA and its uncertainty is influenced by the voltage and rotate speed of CPMA (Olfert and Collings, 2005).

635 In practice, the uncertainty can be determined through setting the resolution ( $R_m$ ) parameter of CPMA. CPMA can change the voltage and rotate speed automatically to meet the uncertainty which was ~10% during our experiment.

The uncertainty of  $D_{mob}$  has been determined to be ~3% (Kinney et al., 1991). The uncertainty of  $M_{rBC}$  has determined to be ~30% (Shiraiwa et al., 2008).

640 For particle density, from the equation

$$\rho_{eff} = \frac{6M_p}{\pi D_{mob}^3} \quad (1)$$

Applying the propagation of uncertainty gives:

$$\left(\frac{\varepsilon_{\rho}}{\rho}\right)^2 = \left(\frac{\varepsilon_{M_p}}{M_p}\right)^2 + 9\left(\frac{\varepsilon_{D_{mob}}}{D_{mob}}\right)^2$$

Then the uncertainty of  $\rho$  was determined to be 13.5%.

For dynamic shape factor, from the equation

$$\chi = \frac{D_{mob} \times C_c(D_{mev})}{D_{mev} \times C_c(D_{mob})} \quad (2)$$

Applying the propagation of uncertainty gives:

$$\left(\frac{\varepsilon_{\chi}}{\chi}\right)^2 = \left(\frac{\varepsilon_{D_{mob}}}{D_{mob}}\right)^2 + \left(\frac{\varepsilon_{D_{mev}}}{D_{mev}}\right)^2 + 2\left(\frac{\varepsilon_{C_c}}{C_c}\right)^2 \quad (3)$$

650 the  $\varepsilon_{C_c}/C_c$  is the same for all particle sizes and equals to 2.1% (Allen and Raabe, 1985). The  $D_{mev}$  is derived from equation 4-5 and the  $\varepsilon_{D_{mev}}/D_{mev}$  is calculated to be ~4% .

$$M_p = \frac{\pi}{6} (D_{mev}^3 - D_c^3) * \rho_{coat} + \frac{\pi}{6} D_c^3 * \rho_{rBC} \quad (4)$$

$$D_{mev} = \sqrt[3]{\frac{6}{\pi} (M_p - \left(1 - \frac{\rho_{coat}}{\rho_{rBC}}\right) * M_{rBC})} \quad (5)$$

Then, the uncertainty of  $\chi$  was determined to be 5.8%.

For void ratio,

$$R_{void} = 1 - \frac{D_{mev}^3}{D_{mob}^3} \quad (6)$$

$$\left(\frac{\varepsilon_{R_{void}}}{R_{void}}\right)^2 = 9 \left(\frac{\varepsilon_{D_{mob}}}{D_{mob}}\right)^2 + 9 \left(\frac{\varepsilon_{D_{mev}}}{D_{mev}}\right)^2 \quad (7)$$

Then, the uncertainty of  $R_{void}$  was determined to be 19.6%.

For mass ratio ( $M_R$ )

$$M_R = \frac{M_p - M_{rBC}}{M_{rBC}} \quad (8)$$

$$\left(\frac{\varepsilon_{M_R}}{M_R}\right)^2 = \left(\frac{\varepsilon_{M_p}}{M_p}\right)^2 + \left(\frac{\varepsilon_{M_{rBC}}}{M_{rBC}}\right)^2 \quad (9)$$

Then, the uncertainty of  $M_R$  was determined to be 31.6%.

Allen, M. D., and Raabe, O. G.: Slip Correction Measurements of Spherical Solid Aerosol-Particles in an Improved Millikan Apparatus, *Aerosol Science and Technology*, 4, 269-286, Doi 10.1080/02786828508959055, 1985.

670 Bond, T. C., Doherty, S. J., Fahey, D., Forster, P., Berntsen, T., DeAngelo, B., Flanner, M., Ghan, S., Kärcher, B., and Koch, D.: Bounding the role of black carbon in the climate system: A scientific assessment, *Journal of Geophysical Research: Atmospheres*, 118, 5380-5552, 2013.

Kinney, P. D., Pui, D. Y. H., Mulholland, G. W., and Bryner, N. P.: Use of the Electrostatic Classification Method to Size 0.1  $\mu$ m Srm Particles - a Feasibility Study, *J Res Natl Inst Stan*, 96, 147-176, 10.6028/jres.096.006, 1991.

Olfert, J. S., and Collings, N.: New method for particle mass classification - the Couette centrifugal particle mass analyzer, *J Aerosol Sci*, 36, 1338-1352, 10.1016/j.jaerosci.2005.03.006, 2005.

675 Shiraiwa, M., Kondo, Y., Moteki, N., Takegawa, N., Sahu, L., Takami, A., Hatakeyama, S., Yonemura, S., and Blake, D.: Radiative impact of mixing state of black carbon aerosol in Asian outflow, *Journal of Geophysical Research: Atmospheres*, 113, 2008.



**Reply to the comments of anonymous reviewer #1 on manuscript  
Entitled " Effective densities of soot particles and their relationships with the mixing state  
at an urban site of the Beijing mega-city in the winter of 2018"**

685 We appreciate very much for the insight comments and recommendations of the reviewer in improving this paper and our future research. Here, we will response to all the comments one by one as follows:

1. Measurement procedures (Section 2.2) Aerosol particles were measured in the six steps using DMA-CPMA tandem system. In analytical condition, it took 10 minutes for each step (whole scan needs one hour). What is the response to  
690 achieve equilibrium in step change? Usually, data after equilibrium condition were used in the stepwise measurements to reduce analytical errors. In other words, data immediately after step change were not suitable for analysis.

Reply: Yes, what the reviewer concerned is exactly right. The residence time between CPMA and SP2 is calculated to be ~19 s. Thus, the first 19 s in each step is easily influenced by the aerosols in the last step. In actual data analyze in this study, to carefully ensure the reliability of the data, the data in first 1 minute but not just 19 s of each step is abandoned.

695

2. Refractive index (Section 2.3.2) Refractive index of  $1.48 + 0i$  was used for measurements of optical diameter. What is aerosol components with refractive index of  $1.48 + 0i$ ? This information is helpful for readers who are not familiar with aerosol optical properties.

Reply: The refractive index of  $1.48 + 0i$  is the representative refractive index of ambient aerosols (mixture of various  
700 components) and always used in the optical diameter calculation (Subramanian et al., 2010;Liu et al., 2014). Taylor et al. (2015) used the relative contribution of organics, nitrate and sulfate measured by SP-AMS to calculate the time-dependent refractive index of ambient aerosols and got the value of 1.46-1.50 (mean 1.48). They reported this refractive index is dominant by organics which is just similar to our cases. We will add the reference of (Taylor et al., 2015) to the refractive index of 1.48.

705 Also, as mentioned in the manuscript (line 201-203), the refractive indices of major components are reported for readers who are not familiar with optical properties as a reference.

3. Line 177-180 Effective density of non-rBC with  $0.8-1.2 \text{ g cm}^{-3}$  (brue, yellow, and red) was no 20 % during EPs 1 and 5. The density was 30-40 % during EPs 1 and 5 in Fig. 1.

710 Reply: Thanks for the reminding. We have checked the data, the density was 20-40 % during the EPs 1 and 5 in Fig. 1. We will change the number in the next version. However, this change don't influence the result since 20-40 % is still significantly lower than ~70% in EPs 2 and 4.

715 4. Line 206-207 and Fig. 2 Figure 2 provides us very important and interesting knowledge on relation between aerosol size and effective density. Before detail discussion, influence of analytical error should be discussed. It is true that variation of refractive index can influence optical diameter. However, analytical error or analytical precision in the tandem system needs to be taken into account.

Reply: A detailed uncertainty analyze was conducted in the supplementary.

720 For the optical size exhibited in Fig. 2. It's transformed from the scattering signal directly measured by SP2. The scatter of the distribution intensity of scattering can cause ~4% uncertainty of the optical diameter. The DMA-CPMA tandem system can cause ~3% uncertainty of the mobility diameter. However, the different choosing of refractive indices can cause up to ~14% uncertainty of the optical diameter. Thus, we mainly discuss about the uncertainty caused by the refractive indices.

725 5. Line 247-250 Rvoid value (0.92) was shown in this sentence. In Figure 3, Rvoid of 0.92 seems to be too large. Is that typo?

Reply: Yes, it's just a typo. 0.92 is actually the value of Rno\_void, and the value of Rvoid is 0.08. We will change the number in the next version. We appreciate the reviewer pointed out this mistake.

730 6. Line 307-309 As shown in the text, insufficient detection limit can lead to disturb identification of detection of bi-modal pattern. Also, low analytical resolution in density may be one of the reasons.

735 Reply: The low analytical resolution may be truly one of the reasons. We will change the sentence to "We speculate that the  $\rho_{\text{rBC}}$  number distribution will exhibit a bimodal pattern if the detection limit is sufficiently low and the analytical resolution is sufficiently high. The left peak in the expected bimodal pattern corresponds to the rBC-containing particles with thin coatings." (Line 287-289)

7. Line 322-326 This difference between Eps 2 &4 and Eps 1 & 5 is very interesting in comparison of ambient aerosols. Are there any differences in meteorological conditions, air mass history, and so on? What were important or key processes to engender the differences?

740 Reply: We also found the difference between EPs 2&4 and EPs 1&5 which is very interesting. The air mass history didn't show distinct differences as shown in Fig. S5. We suspected the different meteorological conditions during these episodes leading to the different formation processes of aerosols (more organics in EPs 2&4). However, we think the major purpose of this paper is to explore the relationship between density and rBC's mixing state. Thus, we would like to investigate deeper

in the next study to figure out the relationship among meteorological conditions, aerosols components and effective  
745 densities.

8. Figures 5-7 Analytical errors (i.e., error bars) should be added in the plots.

Reply: For Fig. 5, what we want to exhibit is the number distribution of rBC-containing particles and non-rBC with different  
effective densities. We think an error bar may be not necessary for such number distribution figures.

750 For Fig. 6, there have been an error bar in the figure.

For Fig. 7, we have added a new error bar denotes the analytical errors of the measured scattering cross section by SP2.

755 Liu, D., Allan, J. D., Young, D. E., Coe, H., Beddows, D., Fleming, Z. L., Flynn, M. J., Gallagher, M. W., Harrison, R. M., Lee,  
J., Prevot, A. S. H., Taylor, J. W., Yin, J., Williams, P. I., and Zotter, P.: Size distribution, mixing state and source apportionment  
of black carbon aerosol in London during wintertime, *Atmospheric Chemistry and Physics*, 14, 10061-10084, 10.5194/acp-  
14-10061-2014, 2014.

760 Subramanian, R., Kok, G. L., Baumgardner, D., Clarke, A., Shinozuka, Y., Campos, T. L., Heizer, C. G., Stephens, B. B., de  
Foy, B., Voss, P. B., and Zaveri, R. A.: Black carbon over Mexico: the effect of atmospheric transport on mixing state, mass  
absorption cross-section, and BC/CO ratios, *Atmospheric Chemistry and Physics*, 10, 219-237, 10.5194/acp-10-219-2010,  
2010.

Taylor, J. W., Allan, J. D., Liu, D., Flynn, M., Weber, R., Zhang, X., Lefer, B. L., Grossberg, N., Flynn, J., and Coe, H.:  
Assessment of the sensitivity of core/shell parameters derived using the single-particle soot photometer to density and  
refractive index, *Atmos Meas Tech*, 8, 1701-1718, 10.5194/amt-8-1701-2015, 2015.

765 **Reply to the comments of anonymous reviewer #2 on manuscript**  
**Entitled " Effective densities of soot particles and their relationships with the mixing state**  
**at an urban site of the Beijing mega-city in the winter of 2018"**

770 We appreciate very much the insight comments and recommendations of the reviewer in improving this paper and our future research. Here, we will response to all the comments one by one as follows:

General comments:

775 While the authors are fully aware that rBC particles in ambient air range in their effective densities from as low as 0.3 g/cm<sup>3</sup> (see Page 8 Line 230 and references therein), they arbitrarily set the lowest limit of detection to 0.8 g/cm<sup>3</sup>, thus giving up a sizable fraction of rBC particles in ambient air. This makes their conclusions truncated that need to be supplemented with extrapolation and to some extent speculations. Why did they do this? One might presume that by setting the mobility diameter to 240 nm they perhaps thought that native (freshly emitted) rBC particles having very low effective densities are not relevant in this range?

Reply:

780 The initial purpose of this experiment is to investigate the relationship between the morphology of rBC-containing particles with their mixing state. The rBC-containing particles with different effective densities are representative of rBC-containing particles with different morphology. Thus, in the experiment design, we focus on the rBC-containing particles with relatively large effective density which have the opportunity to transform from a fractal structure to spherical structure. However, we admit we ignore the rBC-containing particles with less effective density and cannot show a whole spectrum of effective density distribution which was not our initial purpose of our experiment. Besides, there is actually a balance which need to be considered in a DMA-CPMA-SP2 measurement. As shown in Figure. 1 below, the detect efficiency (denoted by SP2/CPC) was not 100% for small rBC-containing particles ( $M_p < 4$  fg). The lower detection limit of this study is effective density of 0.8 g/cm<sup>3</sup> corresponding to  $M_p = 5.79$  fg. A lower effective density bound would cause large bias due to the detection limit of SP2. One solution is to increase the mobility diameter selected by DMA. However, another problem exists, since rBC-containing particle mainly locates in the small size range. The increasing in size of rBC-containing particles will significantly decrease the number detected by SP2 which will cause a big problem in the data interpretation especially in clean episodes when the number concentration of rBC-containing particle was typically low. For these two reasons, we decided a detection limit of 0.8 g/cm<sup>3</sup> which may miss the fresh emitted rBC-containing particles.

790 After this experiment, we are also very interested in the whole spectrum of the effective density of rBC-containing particles.  
795 We have thought about some ideas about addressing the problems we mentioned above and will conduct another experiment mainly focus on the whole spectrum of effective density of rBC-containing particles in this winter.

Although some results are from speculations, we think it is reasonable. And some results are quite certain which can help to understand the properties of rBC. For example, we found rBC-containing particles will transform to a near spherical structure when  $M_R > 7$ . Besides, different cases were captured during this experiment including polluted and clean episodes and different polluted type (EP 2&4 and EP 1&5). We think such data is also very precious since the results concluded from such data can be more common.

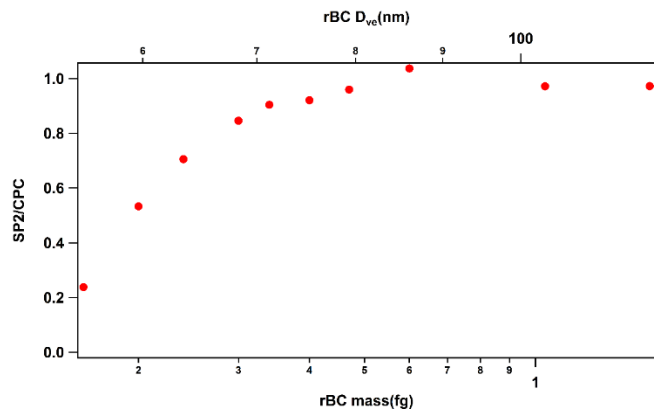


**Figure 1 SP2's detection efficiency of Aquadag.**

805

2) In spite of the fact that several important physical parameters used in this study are derived by subtraction and division of measured quantities that were obtained by fundamentally different techniques (e.g. equations 4 and 5), the authors pay little if any attention to (propagated) uncertainties that can be huge in these cases.

Reply: We will add the uncertainties analyze in the supplementary. The uncertainties of the major parameters used in this

810 paper are discussed.

Detailed comments:

Page 2 Line 37 'glacier reduction' is an imprecise term. Reduction in what? length? volume? albedo? and how? Sea ice and snow albedo is also reduced and melt is affected directly (e.g. by albedo reduction) and indirectly (e.g. by affecting radiative balance over reflective surfaces by absorbing reflected radiation)

815

Reply: Thanks for the reminding of the reviewer. Since BC can influence the glacier in multiple ways such as albedo, volume through direct and indirect effect. We would change "glacier reduction" to "glacier" in the next version. Since this sentence is only aimed to provide a background and emphasize the importance of BC, we don't want to extend and discuss more.

820

Page 2 Line 38 Second most important warming agent. There is no consensus yet whether methane or rBC comes second. Reference outdated, please update references and modify the statement accordingly

Reply: we have changed the expression and reference to “rBC is considered to be one of the most important global warming factors.(Bond et al., 2013).”

825

Page 2 Line 40 ‘Visibility degradation’ is not a major effect of rBC, it is mostly due to scattering aerosols. It is not the human respiratory system that is directly ‘harmed’, but soot has many adverse health effects (including cardiovascular illnesses, cancer, and even brain damage)

830 Reply: We agree with the reviewer and change the expression as well as the reference to “Additionally, as a component of PM<sub>2.5</sub> (particulate matter with an aerodynamic diameter less than 2.5 μm), rBC has an adverse environmental effect by harming human health leading to respiratory and cardiovascular illnesses as well as cancer (Apte et al., 2015;Lelieveld et al., 2015;Raaschou-Nielsen et al., 2013;Dominguez-Rodriguez et al., 2015).” (line 39-41)

835 Page 2 Line 44 ‘other complicated processes’: heterogeneous chemistry, including cloud processing is of utmost importance in affecting the mixing state of submicron particles, it should be mentioned separately

Reply: Great thanks for the reviewer’s reminds. We will add “heterogenous chemistry” separately in the next version. (line 43)

840 Page 2 Line 54 ‘minimize the estimate’? minimize the error in the estimation: : :

Reply: Thanks, we have changed the expression. (line 52-53)

Page 2 Line 82 ‘substantial presence’ please rephrase

845 Reply: The expression has been changed to “Investigation on the peff of rBC-containing particles using a DMA-CPMA-CPC tandem system would be difficult because there are substantial non-rBC particles in the ambient atmosphere.” (line 78-80)

Page 4 Line 103 ‘principal’?

Reply: It’s a typo, we have changed “principal” to “principle”. (line 100)

850 Page 4 Line 105 ‘emits incandescence’ please rephrase

Reply: We have changed the expression to “Then, the rBC is heated to incandescence.” (line 102-103)

Page 5 Line 148-149 flaws in logics: here morphology and properties of BC is preset for the calculations, while the major objective of the study is to determine both

855 Reply: Firstly, we only assume the core-shell structure to calculate the optical diameter of BC, while the refractive indices are measured by previous research(Taylor et al., 2015;Moteki et al., 2010) but aren’t from assumption. We will change the

expression to reduce misleading. The new expression is “By assuming a core-shell structure and using the refractive indices determine by (Taylor et al., 2015), 1.48 for coating and 2.26-1.26i for rBC core, the  $D_{opt}$  of the rBC-containing particles can also be calculated based on the Mie-scattering theory.” (line 147-149)

860 Secondly, using the core-shell assumption is just a method to study the morphology of rBC-containing particles. As we detailed in line 195-197, we compared the optical diameter with the mobility diameter and found rBC-containing particles with less effective density tended to have a less optical diameter although they had the same mobility diameter. This phenomenon may be caused by more fractal structure of rBC-containing particles with less effective density.

865 Thirdly, in my opinion, the optical diameter is actually a representative of particles' scattering ability in this study. We can also use the core-shell model to calculate the scattering intensity of rBC-containing particle with  $D_{mob}= 240$  nm to compare with the measured scattering intensity of rBC-containing particles with varied effective density. We suppose we will get the same result by doing so.

870 Finally, such a core-shell assumption is always used in previous research to transform scattering intensity to optical diameter of rBC-containing particles (Han et al., 2019;Zhang et al., 2018;Laborde et al., 2013). Our result can also suggest one can't simply regard optical diameter as the actual diameter for rBC-containing particles typically for fresh rBC-containing particles with less effective density.

Page 6 Line 165: uncertainty should be reported here since the two parameters are determined by two principally different methods having their own inherent uncertainties

875 Reply: We add the uncertainty of  $M_R$  in line 165-166 and the uncertainties of the major parameters using in this paper can be found in supplementary.

Page 6 Line 171-172 ‘microgram/cm<sup>3</sup>’ ?

880 Reply: We think “ $\mu$  g/cm<sup>3</sup>” have been widely used in previous research and we want to keep consistent with previous research.

Page 6 Line 175 ‘density’ use plural

Reply: Thanks, we have changed the expression.

885 Page 7 Line 195 this statement is definitely not true. Bulk non-rBC particles should differ from the coatings of rBC due to differences in chemistry of their formations.

Reply: As we can see from Fig. S6, the effective densities of bulk non-rBC tended to be less at the condition when there was more organic fraction in the NR-PM<sub>2.5</sub>. We think, the bulk effective density of non-rBC can reflect the organic fraction in non-rBC particles since the densities of organic compounds tend to be less than that of inorganic compounds.

890 Then, the bulk effective of rBC-containing particles also tended to be less at the condition when there was more organic fraction in the NR-PM<sub>2.5</sub> which may be the result of more organic coating.

Thus, our logic is the less bulk non-rBC effective density represents the more organic fraction condition leading to more organic coating of rBC.

We agree the bulk non-rBC particles should differ from the coatings of rBC due to differences in chemistry of their  
895 formations. However, the simultaneous decrease of the bulk effective densities of non-rBC and rBC-containing particles when organic fraction increased (Fig. S6) suggests there was some relationship between the composition of non-rBC and the coating of rBC-containing particles. Thus, the bulk effective density of non-rBC can reflect the composition of coatings of rBC in some degree.

For preciseness, we will change “same” to “similar” in the manuscript. (line 195)

900

[Page 8 Line 243-249 The whole statement is highly speculative \(see my comment immediately above\)](#)

Reply: We have carefully considered the comments of the reviewer. We agree this statement lacks direct evidence, such as the direct measurement of the composition of non-rBC and rBC-containing particles to support the argument. However, we still believe the effective density can reflect the composition of non-rBC and the coating of rBC in some degree. Due to  
905 instrument limits, we are not able to do more experiments to approve this assumption at present. We would like to explore such relationship further in the future.

In this paper, we will weaken the statement about the coating composition effects on rBC. Line 243-249 has been rewritten (now line 240-245).

The former statement: “Since the  $\rho_{rBC}$  was influenced by the combined effect of the coating chemical composition and  
910 morphology, the variation in  $\chi$  and  $R_{void}$  were separately counted in different  $\rho_{non-rBC,bulk}$  situations representing the different coating composition conditions. The rBC-containing particles with a lower coating effective density ( $1.1 < \rho_{non-rBC,bulk} < 1.3 \text{ g/cm}^3$ ) could reach a compact spherical structure when the  $\rho_{rBC}$  was  $1.2 \text{ g/cm}^3$  with an  $\chi$  of 1.05 and a  $R_{void}$  of 0.92, whereas the morphological transition of  $\rho_{rBC}$  was higher for rBC-containing particles at a higher  $\rho_{non-rBC,bulk}$  condition.”

The new version: We found that rBC-containing particle had a larger  $\chi$  value and  $R_{void}$  at the condition when  $\rho_{non-rBC,bulk}$  is  
915 smaller, especially for irregular particles (Fig. 3a). It may imply that different coating composition played a different role in the morphology reconstructing of rBC-containing because  $\rho_{non-rBC,bulk}$  reflected the composition of non-rBC which may relate to the coating composition of rBC in some degree (Fig. S6). The rBC-containing particles could reach a compact spherical structure when the  $\rho_{rBC}$  was  $1.2 \text{ g/cm}^3$  with an  $\chi$  of 1.05 and a  $R_{void}$  of 0.08 when  $1.1 \text{ g/cm}^3 < \rho_{non-rBC,bulk} < 1.3 \text{ g/cm}^3$ , whereas the morphological transition of  $\rho_{rBC}$  was higher for rBC-containing particles at a higher  $\rho_{non-rBC,bulk}$  condition.

920 The former line 270-283 has been deleted.

## Reference

Han, C., Li, S. M., Liu, P., and Lee, P.: Size Dependence of the Physical Characteristics of Particles Containing Refractory

- Black Carbon in Diesel Vehicle Exhaust, *Environ Sci Technol*, 53, 137-145, 10.1021/acs.est.8b04603, 2019.
- 925 Laborde, M., Crippa, M., Tritscher, T., Juranyi, Z., Decarlo, P. F., Temime-Roussel, B., Marchand, N., Eckhardt, S., Stohl, A., Baltensperger, U., Prevot, A. S. H., Weingartner, E., and Gysel, M.: Black carbon physical properties and mixing state in the European megacity Paris, *Atmospheric Chemistry and Physics*, 13, 5831-5856, 10.5194/acp-13-5831-2013, 2013.
- Moteki, N., Kondo, Y., and Nakamura, S.: Method to measure refractive indices of small nonspherical particles: Application to black carbon particles, *J Aerosol Sci*, 41, 513-521, 10.1016/j.jaerosci.2010.02.013, 2010.
- 930 Taylor, J. W., Allan, J. D., Liu, D., Flynn, M., Weber, R., Zhang, X., Lefer, B. L., Grossberg, N., Flynn, J., and Coe, H.: Assessment of the sensitivity of core/shell parameters derived using the single-particle soot photometer to density and refractive index, *Atmos Meas Tech*, 8, 1701-1718, 10.5194/amt-8-1701-2015, 2015.
- Zhang, Y. X., Su, H., Ma, N., Li, G., Kecorius, S., Wang, Z. B., Hu, M., Zhu, T., He, K. B., Wiedensohler, A., Zhang, Q., and Cheng, Y. F.: Sizing of Ambient Particles From a Single-Particle Soot Photometer Measurement to Retrieve Mixing State of Black Carbon at a Regional Site of the North China Plain, *J. Geophys. Res.-Atmos.*, 123, 12778-12795, 10.1029/2018jd028810, 2018.
- 935 Bond, T. C., Doherty, S. J., Fahey, D., Forster, P., Berntsen, T., DeAngelo, B., Flanner, M., Ghan, S., Kärcher, B., and Koch, D.: Bounding the role of black carbon in the climate system: A scientific assessment, *Journal of Geophysical Research: Atmospheres*, 118, 5380-5552, 2013.

940

## Reply to the interactive comments on manuscript

### Entitled " Effective densities of soot particles and their relationships with the mixing state at an urban site of the Beijing mega-city in the winter of 2018"

945

Thanks for the comments, we will response to all the comments one by one as follows:

1. Comment on the representative of rBC particles in this study This paper only focuses on the rBC particles with effective density from 0.8 to 1.8 g cm<sup>-3</sup>. Actually, lots of rBC particles emitted from emission sources show a much lower effective density. Unfortunately, they are not included in this study.

950

Reply: The initial purpose of this experiment is to investigate the relationship between the morphology of rBC-containing particles with their mixing state. The rBC-containing particles with different effective densities are representative of rBC-containing particles with different morphology. Thus, in the experiment design, we focus on the rBC-containing particles with relatively large effective density which have the opportunity to transform from a fractal structure to spherical structure.

955

However, we admit we ignore the rBC-containing particles with less effective density and cannot show a whole spectrum of effective density distribution which was not our initial purpose of our experiment. Besides, there is actually a balance which need to be considered in a DMA-CPMA-SP2 measurement. As shown in Figure. 1 below, the detect efficiency (denoted by SP2/CPC) was not 100% for small rBC-containing particles ( $M_p < 4$  fg). The lower detection limit of this study is effective density of 0.8 g/cm<sup>3</sup> corresponding to  $M_p = 5.79$  fg. A lower effective density bound would cause large bias due to the detection limit of SP2. One solution is to increase the mobility diameter selected by DMA. However, another problem exists, since rBC-containing particle mainly locates in the small size range. The increasing in size of rBC-containing particles will significantly decrease the number detected by SP2 which will cause a big problem in the data interpretation especially in clean episodes when the number concentration of rBC-containing particle was typically low. For these two reasons, we decided a detection limit of 0.8 g/cm<sup>3</sup> which may miss the fresh emitted rBC-containing particles.

965

After this experiment, we are also very interested in the whole spectrum of the effective density of rBC-containing particles. We have thought about some ideas about addressing the problems we mentioned above and will conduct another experiment mainly focus on the whole spectrum of effective density of rBC-containing particles in this winter.

Although some results are from speculations, we think it is reasonable. And some results are quite certain which can help to understand the properties of rBC. For example, we found rBC-containing particles will transform to a near spherical structure when  $M_R > 7$ . Besides, different cases were captured during this experiment including polluted and clean episodes and different polluted type (EP 2&4 and EP 1&5). We think such data is also very precious since the results concluded from such data can be more common.

970

2. Comment on the calculation and definition of effective density This paper presents two methods of effective densities calculation, but I do not quite understand them. Previous studies (Qiao et al., 2018; Momenimovahed and Olfert, 2015) generally used a log-normal or Gaussian function to fit the eff distribution. The eff of the bulk aerosols was determined to be the peak location of the fit function. In this paper, however, the first calculation method (Lines 125-130) is, “Particles with known effective densities preselected by the DMA-CPMA system were injected into the SP2 to obtain information on the corresponding BC. In practice, the mobility diameter selected by the DMA was set at a constant value of 240 nm. The setpoints of the CPMA were 5.79, 7.24, 8.69, 10.13, 11.58, and 13.03 fg, which corresponded to a eff of 0.8,1.0, 1.2, 1.4, 1.6, and 1.8 g/cm<sup>3</sup>, respectively.” This calculation is totally different from the calculation in the previous studies. Is no a log-normal or Gaussian function fitted? It is imprecise in theory and in practice. What is the strategy about the selection of CPMA data? The second calculation method defines a new effective density which names the bulk aerosol density, as stated in Lines 137. In my opinion, it should be the bulk aerosol effective density. Additionally, the authors simply use the PSL to demonstrate this method, which lacks the experiments about rBC.

Reply: We want to emphasize that there are two effective densities in this paper, one is the effective density of a single particle and the other is the effective density of aerosol bulk since aerosol bulk has various aerosols with different effective densities.

The previous studies which we listed is just the method to determine the aerosol bulk effective density and can't be simply compared with the method we select particles with a certain effective density. As a matter of fact, the calculation and the theory of previous research are just similar to our study. What they do is to measure more effective densities points. For example, “the mobility diameter selected by the DMA was set at a constant value of 240 nm. The setpoints of the CPMA were ...,5.79, ..., 7.24, ..., 8.69, ...,10.13, ...,11.58, ...,and, ...,13.03fg, which corresponded to an effective density of 0.5,0.6,0.7,0.8,0.9,1.0,1.1,1.2,1.3,1.4,1.5,1.6,1.7,1.8 g/cm<sup>3</sup>, respectively” in their paper. Thus, with more effective density points, one can fit a log-normal or Gaussian function to determine the peak location of the effective density distribution. The main purpose of such fitting is to find the effective density with the maximum number counts to represent the effective density characteristic of the bulk aerosol. In our study, due to the detection resolution, we adopt a new method whose main purpose is also to find effective density of the maximum number counts. As long as the number counts of each effective density is measured correctly, this method will not cause an uncertainty larger than 0.1 g/cm<sup>3</sup> in the determination of the eff of the bulk effective density in our study.

3. Comment on the setup of DMA-CPMA-SP2 This study uses a novel setup to characterize the effective density of rBC particles in the atmosphere, but this setup does not be verified by rBC particles produced in laboratory. I strongly suggest that it should be assessed before applying it to the field observation.

Reply: Yes, this is a good advice and we would like to do so to make our result more convincing. However, there is some trouble with our SP2's flow system now and it can't operate normally.

However, I can give you an evidence in another aspect. We measured the effective density of Aquadag using the DMA-CPMA-CPC system in previous study which showed a good consistency with other researchers (Figure. 1). In DMA-CPMA-SP2 system, we can say surely we can get the same result as DMA-CPMA-CPC system in our previous study, since the function of SP2 is to detect the number of rBC which shows a good consistency with CPC (Figure. 2).

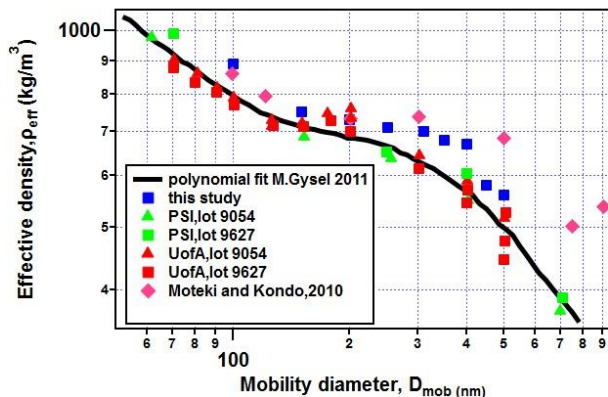


Figure 1 Relationship between effective density and mobility diameter of Aquadag measured by DMA-CPMA-CPC system and in previous studies.

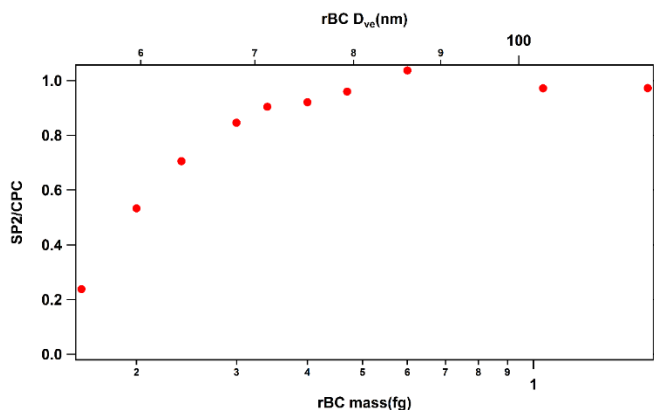


Figure 2 SP2's detection efficiency of Aquadag.

4. Comment on the determination of the shape factor In 2.3.3, author uses the equation (3) to determine the dynamic shape factor. In the equation,  $D_{mev}$  is the mass equivalent diameter. The authors do not explain how the value of this mass equivalent diameter is obtained. According to the instruments used in this paper, it seems impossible to obtain  $D_{mev}$ . I am confused that this paper has calculated dynamic shape factor by the value of  $D_{mev}$ .

Reply: The  $D_{mev}$  is calculated by solving the following equation:

$$M_{coat} = \left( \frac{1}{6} * \pi * D_{mev}^3 - \frac{1}{6} * \pi * D_c^3 \right) * \rho_{coat} = M_p - M_{rBC}$$

$\rho_{coat}$  is assumed to be the same as  $\rho_{non-rBC,bulk}$  in this study. (see the response to the anonymous reviewer #2)

